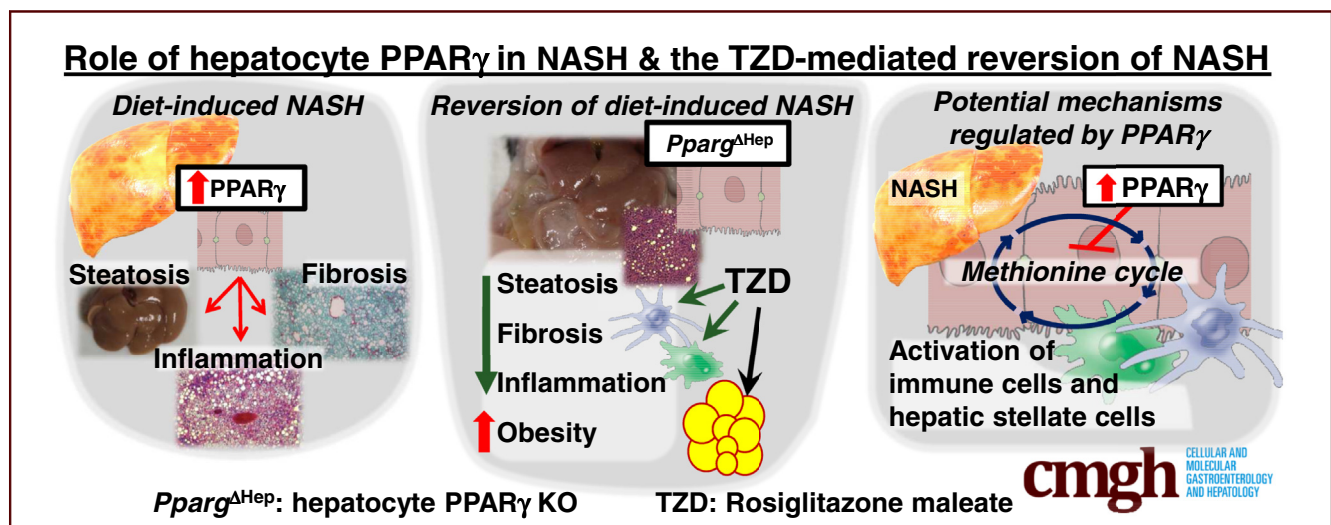# ORIGINAL RESEARCH

Hepatocyte-Specific Loss of PPARγ Protects Mice From NASH and Increases the Therapeutic Effects of Rosiglitazone in the Liver

Samuel M. Lee,[1] Carolina M. Pusec,[1] Gregory H. Norris,[1] Adam De Jesus,[2] Alberto Diaz-Ruiz,[3] Jose Muratalla,[1] Andre Sarmento-Cabral,[1] Grace Guzman,[4] Brian T. Layden,[1,5] and Jose Cordoba-Chacon[1]

[1]Department of Medicine, Division of Endocrinology, Diabetes and Metabolism, University of Illinois at Chicago, Chicago, Illinois; [2]Northwestern University, Chicago, Illinois; [3]IMDEA-Food, Madrid, Spain; [4]Department of Pathology, University of Illinois at Chicago, Chicago, Illinois; and [5]Research and Development, Jesse Brown VA Medical Center, Chicago, Illinois

Role of hepatocyte PPARγ in NASH & the TZD-mediated reversion of NASH

Diet-induced NASH — ↑PPARγ — Steatosis, Fibrosis, Inflammation

Reversion of diet-induced NASH — Pparg^ΔHep — ↓Steatosis, Fibrosis, Inflammation, ↑Obesity — TZD

Potential mechanisms regulated by PPARγ — NASH — ↑PPARγ — Methionine cycle — Activation of immune cells and hepatic stellate cells

Pparg^ΔHep: hepatocyte PPARγ KO   TZD: Rosiglitazone maleate

SUMMARY

The efficacy of TZD on resolving liver pathology is limited, and that could be due to the activation of peroxisome proliferator-activated receptor gamma (PPARγ) in hepatocytes. By knocking out hepatocyte-specific PPARγ in mice, we explored the pathogenic role of this receptor in the development of NASH in the presence of TZD, revealing novel mechanisms in NASH.

BACKGROUND & AIMS: Nonalcoholic steatohepatitis (NASH) is commonly observed in patients with type 2 diabetes, and thiazolidinediones (TZD) are considered a potential therapy for NASH. Although TZD increase insulin sensitivity and partially reduce steatosis and alanine aminotransferase, the efficacy of TZD on resolving liver pathology is limited. In fact, TZD may activate peroxisome proliferator-activated receptor gamma (PPARγ) in hepatocytes and promote steatosis. Therefore, we assessed the role that hepatocyte-specific PPARγ plays in the development of NASH, and how it alters the therapeutic effects of TZD on the liver of mice with diet-induced NASH.

METHODS: Hepatocyte-specific PPARγ expression was knocked out in adult mice before and after the development of NASH induced with a high fat, cholesterol, and fructose (HFCF) diet.

RESULTS: HFCF diet increased PPARγ expression in hepatocytes, and rosiglitazone further activated PPARγ in hepatocytes of HFCF-fed mice in vivo and in vitro. Hepatocyte-specific loss of PPARγ reduced the progression of HFCF-induced NASH in male mice and increased the benefits derived from the effects of TZD on extrahepatic tissues and non-parenchymal cells. RNAseq and metabolomics indicated that HFCF diet promoted inflammation and fibrogenesis in a hepatocyte PPARγ–dependent manner and was associated with dysregulation of hepatic metabolism. Specifically, hepatocyte-specific loss of PPARγ plays a positive role in the regulation of methionine metabolism, and that could reduce the progression of NASH.

CONCLUSIONS: Because of the negative effect of hepatocyte PPARγ in NASH, inhibition of mechanisms promoted by endogenous PPARγ in hepatocytes may represent a novel strategy that increases the efficiency of therapies for NAFLD.

The prevalence of nonalcoholic fatty liver disease (NAFLD) is 25% in the general population and can be as high as 80% in patients with type 2 diabetes.[1,2] The main pathologic features of NAFLD are hepatic steatosis and insulin resistance. Nonalcoholic steatohepatitis (NASH) is an advanced pathologic state of NAFLD that is characterized by severe inflammation, hepatocyte ballooning, and liver damage in the presence or absence of fibrosis.[3] Only a small percentage of patients with NAFLD progresses to NASH, but in those with type 2 diabetes, the progression to NASH is 10 times higher (37%) than in the general population.[2] Although NAFLD and NASH are reversible conditions, the multiple mechanisms that promote this disease and the lack of a Food and Drug Administration–approved medical treatment make NAFLD a significant burden on the healthcare system.

Because insulin resistance is a common feature in the pathogenesis of diabetes and NAFLD, thiazolidinediones (TZD), a class of insulin sensitizing drugs used as second-line oral therapy for diabetes, have been tested for their ability to reduce and reverse NAFLD.[4–7] In extrahepatic tissues, TZD activate peroxisome proliferator-activated receptor gamma (PPARγ), increase the sensitivity to insulin, and redirect lipids away from the liver.[8,9] In addition, TZD activate PPARγ in hepatic macrophages and hepatic stellate cells, thereby reducing inflammation and fibrosis, respectively.[10] In clinical trials, TZD have consistently improved insulin sensitivity, steatosis, and plasma alanine aminotransferase (ALT) levels in NASH patients, but with only modest improvement in liver histology.[4–7] Although TZD are effective in reducing insulin resistance and improving glucose control of diabetic subjects, it is not clear why these actions do not translate directly into improved histologic features of NAFLD.

The expression of PPARγ is low in the lean liver as compared with that of muscle and adipose tissue.[9] However, hepatic PPARγ expression increases in patients with steatosis and steatohepatitis,[11,12] and several reports identified PPARγ-regulated hepatic genes and pathways as relevant mechanisms involved in the development of NAFLD.[13–15] In fact, we and others have shown that hepatocyte PPARγ promotes steatosis in mice fed a high fat diet because it increases de novo lipogenesis (DNL) and fatty acid uptake in hepatocytes.[16–20] These mechanisms are associated with the development of liver injury and progression to NAFLD.[3] Because of the positive association between hepatocyte PPARγ and the steatogenic mechanisms that could promote NASH, we hypothesized that the therapeutic actions of TZD on NAFLD patients are diminished by the TZD-mediated activation of PPARγ in hepatocytes. To test our hypothesis, we knocked out the *Pparg* gene in adult hepatocytes before and after dietary-induced NASH. Our results highlight that hepatocyte-specific loss of PPARγ protects mice from NAFLD and increases the benefits derived from the effects of TZD on extrahepatic tissues and non-parenchymal cells of the liver.

Results

Hepatocyte-Specific Loss of PPARγ Protects Mice From High Fat, Cholesterol, and Fructose Diet–Induced NASH

Adult-onset hepatocyte-specific PPARγ knockout (*Pparg*$^{\Delta Hep}$) mice were generated by using 10-week-old chow-fed *Pparg*$^{fl/fl}$ mice with adeno-associated virus (AAV)-delivered Cre recombinase, whereas *Pparg*$^{fl/fl}$ mice treated with AAV-Null vector served as controls (see Methods). Two weeks later, a subset of mice in each group was fed a high fat, cholesterol, and fructose (HFCF) diet for 24 weeks to induce NASH[21] or a nutrient-matched low fat, cholesterol, and fructose (LFCF) diet. In male but not female mice, HFCF diet increased the expression of hepatic PPARγ, whereas *Pparg*$^{\Delta Hep}$ reduced and prevented the HFCF-mediated up-regulation of hepatic PPARγ expression (Figure 1*A*). These data suggest that the increase in PPARγ expression observed in fatty liver is largely attributed to increased expression of PPARγ in hepatocytes. HFCF diet increased plasma ALT and liver weight in male mice, whereas liver triglycerides (TG) were increased in both male and female mice (Figure 1*B*). Because of the reduced impact of HFCF diet on plasma ALT, liver weight, and hepatic PPARγ expression in female mice, we scored the development of NASH only in male mice. The NAFLD Activity Score (NAS) of HFCF-fed male control mice was 6.61 ± 0.36, which confirmed the development of NASH, whereas NAS was significantly reduced in HFCF-fed *Pparg*$^{\Delta Hep}$ mice (Figure 1*C*). Specifically, *Pparg*$^{\Delta Hep}$ mice showed reduced steatosis, inflammation, plasma ALT levels, liver weight, liver TG content, and reduced bridging fibrosis (61% of control mice vs 25% of *Pparg*$^{\Delta Hep}$ mice; Figure 1*B–F*), which suggests hepatocyte PPARγ plays a role in the pathogenesis of NASH.

Next, we assessed whether *Pparg*$^{\Delta Hep}$ improved peripheral metabolism and glucose homeostasis to reduce HFCF-induced NASH. Although HFCF diet has a higher energy content than LFCF diet (Supplementary Data), it did not induce obesity in male or female mice. In the groups of
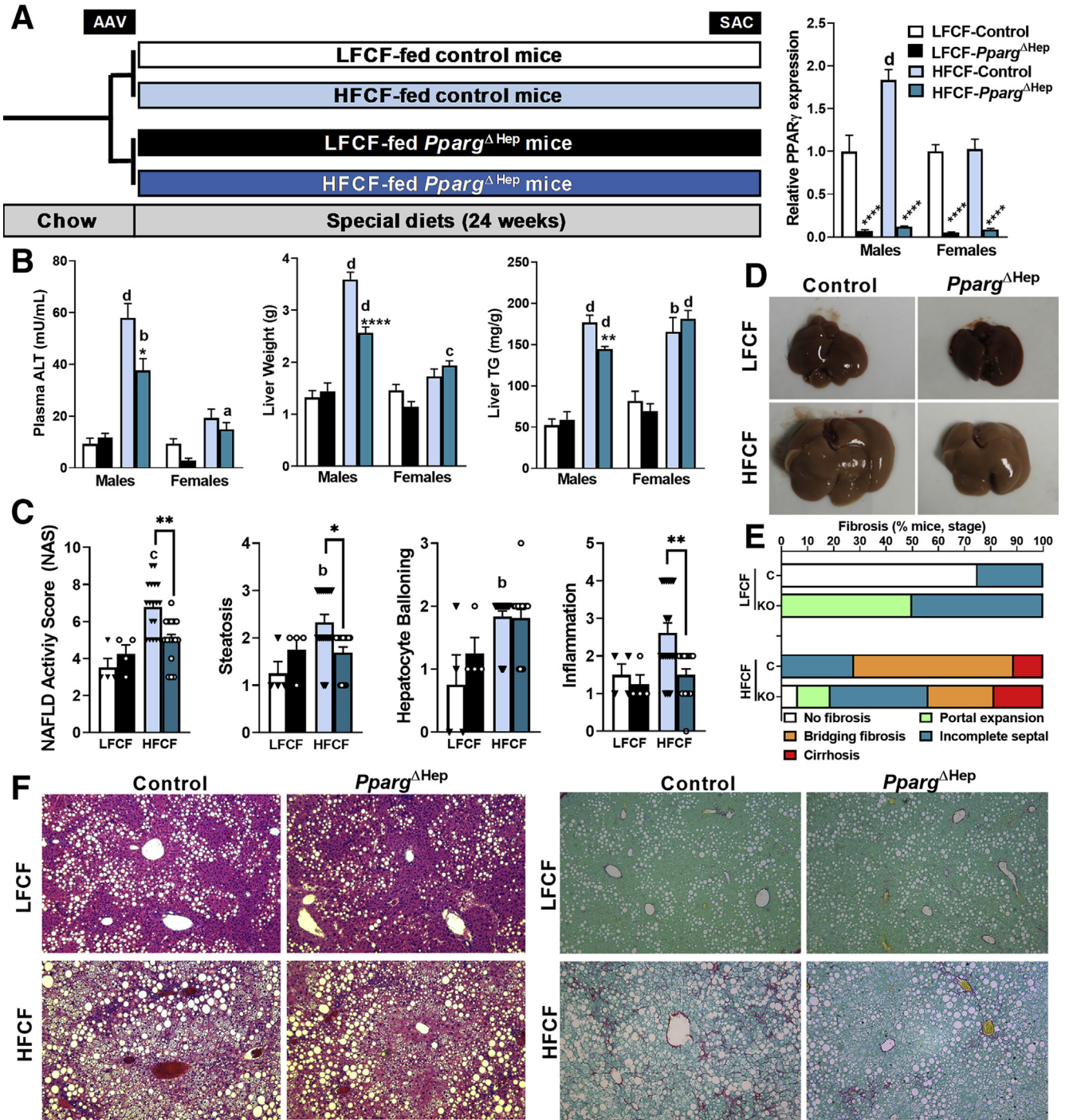
Most current article

Figure 1. Hepatocyte PPARγ promotes NASH in male mice. (*A*) 10-week-old mice were treated with AAV to generate control and *Pparg*[ΔHep] mice, and 2 weeks later these mice were fed the LFCF or HFCF diet for 24 weeks, where quantitative polymerase chain reaction confirmed knockdown of hepatic PPARγ expression (*right*). (*B*) Plasma ALT levels, liver weight, and liver TG content in male and female control and *Pparg*[ΔHep] mice. (*C*) NAS, steatosis, hepatocyte ballooning, and inflammation grade; (*D*) representative pictures of livers; (*E*) percentage of mice by fibrosis stage; and (*F*) representative pictures (original magnification, ×10) of liver sections stained with hematoxylin-eosin (*left*) and picrosirius red/fast green (*right*). *Letters* indicate significant differences between LFCF-fed and HFCF-fed mice within group (C or KO), and *asterisks* indicate significant differences between control and *Pparg*[ΔHep] mice within diet. *$P < .05$; [b,]**$P < .01$; [c,]***$P < .001$; [d,]****$P < .0001$. n = 7–18 mice/group.

mice used to assess metabolic rate and pyruvate tolerance tests, HFCF diet reduced nuclear magnetic resonance (NMR)–based fat mass in control mice (Figures 2A and 3A), but in the groups used to assess glucose and insulin tolerance tests, it did not reduce body weight (Figure 4). The resistance to increase body weight in HFCF-fed mice may be due to increased energy expenditure and utilization of fat as source of energy. Specifically, after 8 weeks of diet, HFCF diet increased energy expenditure and food intake and impaired the circadian shift in the use of metabolic fuel, as indicated by the diurnal oscillations of the respiratory exchange ratio (Figures 2B, 3B, and 5, *left panels*). Although HFCF diet did not alter glucose levels or whole-body insulin sensitivity, it increased insulin levels and liver steatosis and promoted glucose intolerance associated with increased levels of glucose after pyruvate injection (Figures 2C, 3C, and 6; Table 1). The effect of HFCF diet on the metabolic phenotype was lost after 24 weeks of HFCF diet in both male and female mice, with the exception of the increased levels of glucose after pyruvate injection (Table 1; Figures 2D and E, 3D and E). Interestingly, HFCF-fed $Pparg^{\Delta Hep}$ mice showed reduced activity and increased adiposity and insulin levels in males and glucose intolerance in male and female mice as compared with HFCF-fed control mice (Figures 2A, D, and E, 3A, D, and E, 4; Table 1). Taken together, these data suggest that HFCF-induced NASH (Figure 1) should be the consequence of the direct effects of the diet on hepatic metabolism rather than the indirect effects of impaired whole-body metabolism or insulin resistance (Figures 2–6). Importantly, because HFCF-fed $Pparg^{\Delta Hep}$ mice showed protection against HFCF-induced NASH (Figure 1) but concomitant increases in adiposity and impaired glucose homeostasis when compared with HFCF-fed control mice, our results indicate that hepatocyte PPARγ regulates relevant biological processes in the liver promoting NASH.

Hepatocyte PPARγ Regulates Hepatic Metabolism Associated With the Progression of NASH

To further investigate how $Pparg^{\Delta Hep}$ prevents the progression of NASH, we performed RNAseq and metabolomics of liver samples of male mice fed the LFCF and HFCF diets for 24 weeks. HFCF diet altered the expression of 2145 hepatic genes in control mice and only 397 genes in $Pparg^{\Delta Hep}$ mice (Figure 7A). A list of the top differentially expressed genes (DEGs) is provided in Supplementary Data, and the statistical analysis of the DEGs between groups is published in the Gene Expression Omnibus with the accession #GSE162249. The enrichment analysis of these DEGs showed that gene ontology (GO) terms related to inflammation and fibrogenesis and KEGG pathways related to focal adhesion and extracellular matrix–receptor interaction were up-regulated by HFCF diet. Also, GO terms related to mitochondrial function and amino acid metabolism and KEGG pathways related to metabolic pathways and oxidative phosphorylation were down-regulated by HFCF diet (Figure 3A, Supplementary Data). Of note, $Pparg^{\Delta Hep}$ only

altered the expression of 5 genes in LFCF-fed mice, but it altered the expression of 2273 genes in HFCF-fed mice. Interestingly, the enrichment analysis showed that in HFCF-fed mice, $Pparg^{\Delta Hep}$ down-regulated inflammation and fibrogenesis and up-regulated mitochondrial function and amino acid metabolism as compared with HFCF-fed control mice (Figure 7B and C, Supplementary Data). We confirmed the positive effect of HFCF diet and the negative effect of $Pparg^{\Delta Hep}$ in the expression of pro-inflammatory (*Tnfa, Mcp1, Trem2*) and pro-fibrogenic (*Col1a1, Mmp13, Timp1*) genes (Figure 7D). Also, we confirmed that hepatocyte PPARγ must be activated in HFCF-fed mice, because the expression of the PPARγ-target genes *Cidea* and *Cidec*[20] was increased by HFCF diet in control mice, and $Pparg^{\Delta Hep}$ blocked this effect (Figure 7D). Overall, these data suggest that HFCF diet has a strong effect on the regulation of hepatic gene expression in mice with intact hepatocyte PPARγ gene, where it promotes processes involved in the development of NASH: inflammation, fibrogenesis, and dysregulation of metabolism.

Untargeted metabolomics consisting of a panel of 189 hydrophilic metabolites showed 41 and 37 metabolites were regulated by HFCF diet in control and $Pparg^{\Delta Hep}$ mice, respectively, which were related with amino acid and pyrimidine metabolism (Supplementary Data). The strong effect of $Pparg^{\Delta Hep}$ on hepatic metabolites of HFCF-fed mice further indicated that amino acid and pyrimidine metabolism was regulated by HFCF diet in a hepatocyte PPARγ-dependent manner (Figure 7E, Supplementary Data). Furthermore, a joint pathway analysis of RNAseq and metabolomics showed that glutathione metabolism, retinol metabolism, and linoleic acid metabolism among other processes were highly regulated by HFCF diet in a hepatocyte PPARγ-dependent manner (Figure 7F). The regulation of these metabolic processes in NASH[22–24] suggests that hepatocyte PPARγ may be a relevant nuclear receptor in the development of HFCF diet-induced NASH.

Hepatocyte-Specific Loss of PPARγ Enhances the Benefits Derived From the Effects of Rosiglitazone on Extrahepatic Tissues and Non-Parenchymal Cells of the Liver of Mice With NASH

To assess whether the expression of hepatocyte PPARγ has an effect in the TZD-mediated reversion of NASH, we fed a cohort of 8- to 10-week-old $Pparg^{fl/fl}$ mice with a HFCF diet for 24 weeks. After induction of NASH with HFCF diet, we generated control and $Pparg^{\Delta Hep}$ mice. A group of $Pparg^{fl/fl}$ littermates served as LFCF-fed controls. Two weeks after generation of control and $Pparg^{\Delta Hep}$ mice, half of the HFCF-fed mice in each group were switched to a HFCF diet containing 50 mg rosiglitazone maleate/kg for additional 8 weeks. In HFCF-fed control mice, the low dose of rosiglitazone used improved insulin sensitivity and glucose clearance and reduced plasma ALT, but it did not reduce liver weight or steatosis (Figure 8A and B). In HFCF-fed $Pparg^{\Delta Hep}$ mice, TZD also improved insulin sensitivity, but
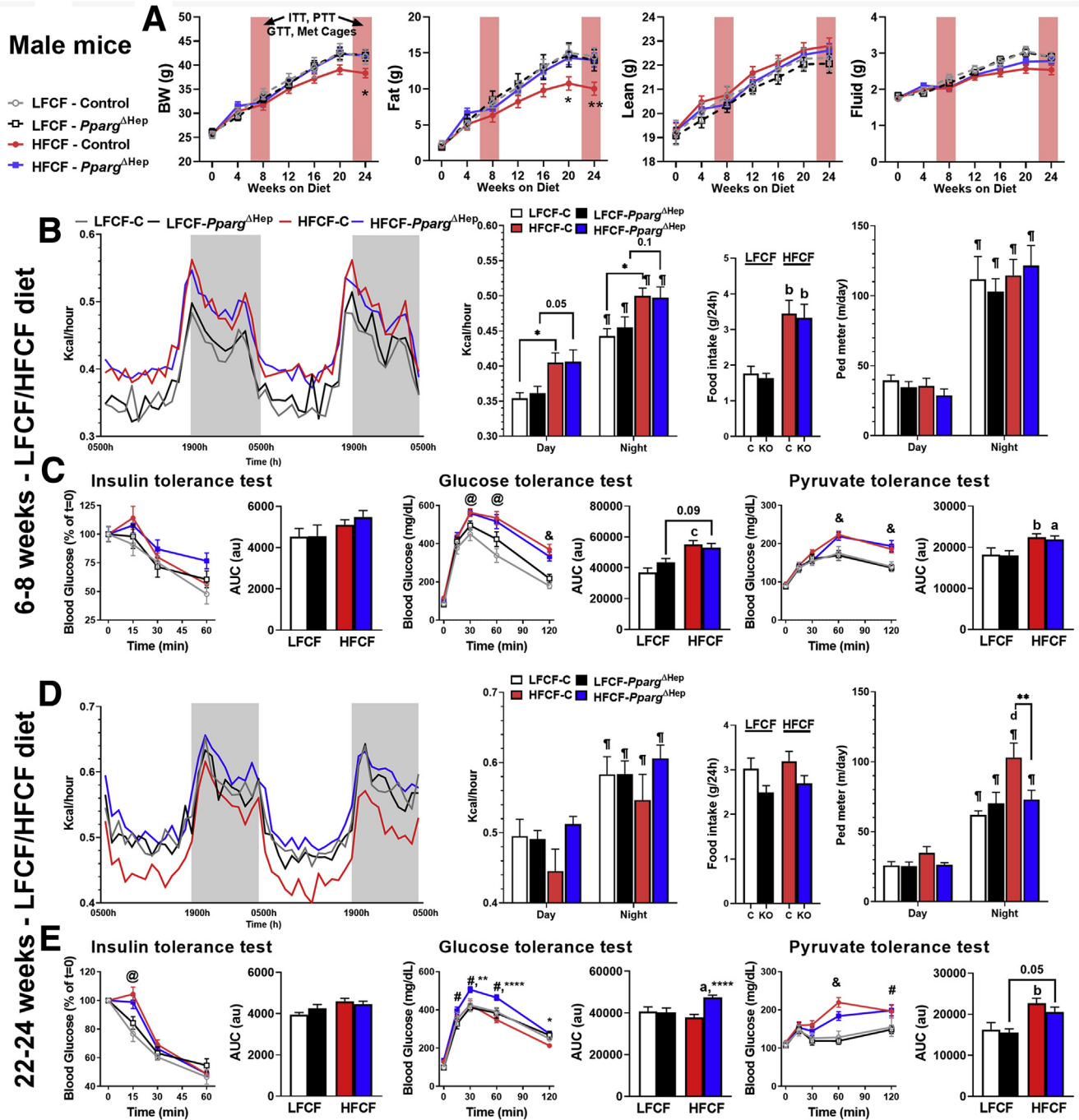
Figure 2. *Pparg*[ΔHep] **did not improve peripheral metabolism or glucose homeostasis in male mice.** (*A*) Body weight and NMR-based fat, lean, and fluid mass of control and *Pparg*[ΔHep] male mice fed the LFCF or HFCF diet for 24 weeks. (*B*) Energy expenditure (48-hour curves and day/night averages), food intake, and day/night average activity after 8 weeks of LFCF and HFCF diets. (*C*) Insulin tolerance test after 6 weeks of diet (*left*), glucose tolerance test after 7 weeks of LFCF/HFCF diet (*middle*), and pyruvate tolerance test after 7 weeks of LFCF/HFCF diet (*right*). (*D*) Energy expenditure (48-hour curves and day/night averages), food intake, and day/night average activity after 24 weeks of LFCF and HFCF diets. (*E*) Insulin tolerance test after 23 weeks of diet (*left*), glucose tolerance test after 23 weeks of LFCF/HFCF diet (*middle*), and pyruvate tolerance test after 22 weeks of LFCF/HFCF diet (*right*). *Letters* (a–d, @, #, &) indicate significant differences between LFCF-fed and HFCF-fed mice within group (control, C and *Pparg*[ΔHep], KO; [@], only C; [#], only KO; [&], C and KO). *Asterisks* indicate significant differences between control and *Pparg*[ΔHep] mice within diet. ¶Significant differences between day and night within groups. [a],*,[@],[#],[&],¶$P < .05$; [b],**$P < .01$; [c],***$P < .001$; [d],****$P < .0001$. AUC, area under the curve. n = 7–18 mice/group. Body composition of the mice used for the GTT and ITT is represented in Figure 4.
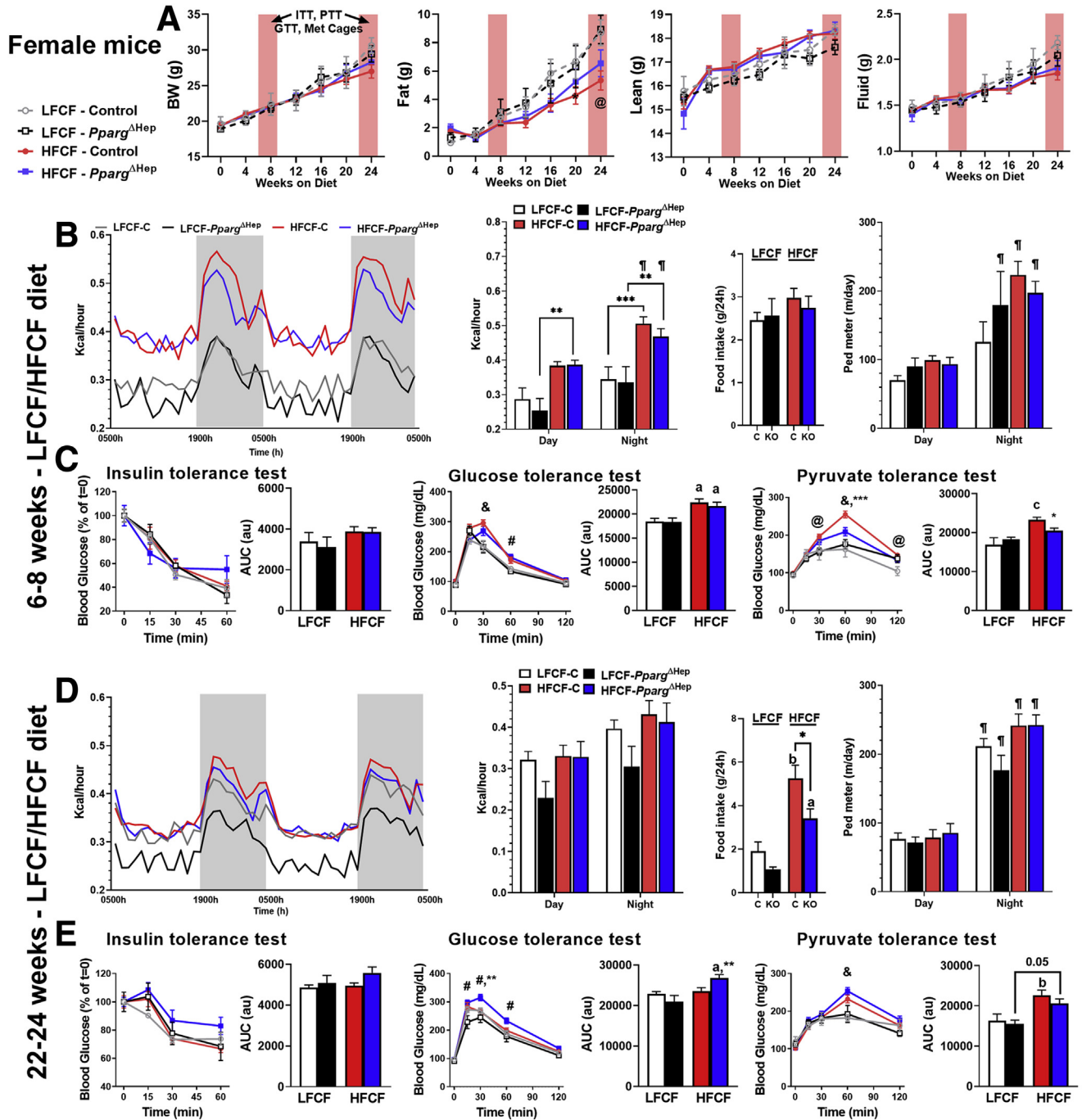
Figure 3. $Pparg^{\Delta Hep}$ **did not improve peripheral metabolism or glucose homeostasis in female mice.** (*A*) Body weight and NMR-based fat, lean, and fluid mass of control and $Pparg^{\Delta Hep}$ female mice fed LFCF or HFCF diet for 24 weeks. (*B*) Energy expenditure (48-hour curves and day/night averages), food intake, and day/night average activity after 8 weeks of LFCF and HFCF diets. (*C*) Insulin tolerance test after 6 weeks of LFCF/HFCF diet (*left*), glucose tolerance test after 7 weeks of LFCF/HFCF diet (*middle*), and pyruvate tolerance test after 7 weeks of LFCF/HFCF diet (*right*). (*D*) Energy expenditure (48-hour curves and day/night averages), food intake, and day/night average activity after 24 weeks of LFCF and HFCF diets. (*E*) Insulin tolerance test after 23 weeks of diet (*left*), glucose tolerance test after 22 weeks of LFCF/HFCF diet (*middle*), and pyruvate tolerance test after 22 weeks of LFCF/HFCF diet (*right*). *Letters* (a–d, @, #, &) indicate significant differences between LFCF- and HFCF-fed mice within group (control, C and $Pparg^{\Delta Hep}$, KO; @, only C; #, only KO; &, C and KO). *Asterisks* indicate significant differences between control and $Pparg^{\Delta Hep}$ mice within diet. ¶Significant differences between day and night within groups. [a],*,[@],[#],[&],¶$P < .05$; [b],**$P < .01$; [c],***$P < .001$; [d],****$P < .0001$. AUC, area under the curve. n = 6–13 mice/group. Body composition of mice used for the GTT and ITT is represented in Figure 4.
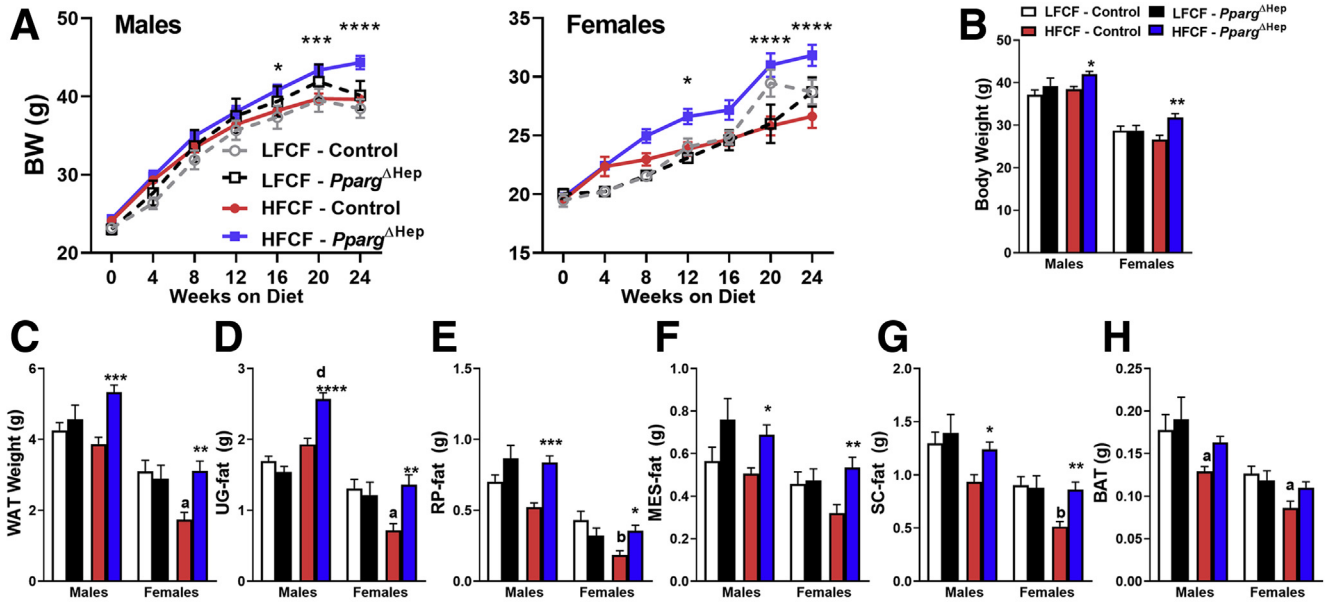
Figure 4. Effect of HFCF diet on adipose tissue weight in control and *Pparg*^ΔHep^ male and female mice. Progression of body weight in male and female mice (*A*). Body weight (*B*) and white adipose tissue (WAT) weight (*C*). WAT is the sum of individual urogenital (UG, *D*), retroperitoneal (RP, *E*), mesenteric (MES, *F*), and subcutaneous (inguinal, SC, *G*) adipose tissue weight of mice fed LFCF or HFCF diet for 24 weeks. Brown adipose tissue (BAT, *D*) weight. Data are represented as means ± standard error of the mean. Data were analyzed by 2-way analysis of variance followed by Bonferroni (*A*) or Tukey (*B–H*) post hoc test. *Letters* indicate significant differences between LFCF- and HFCF-fed mice within group and gender (control, *open columns* and *Pparg*^ΔHep^, *closed columns*). *Asterisks* indicate significant differences between control and *Pparg*^ΔHep^ mice within diet. ^a^,*P < .05; ^b^,**P < .01; ***P < .001; ^d^****P < .0001. n = 6–18 mice/group.

in striking contrast to control mice, TZD promoted glucose intolerance and increased plasma insulin levels (Figure 8*A*, Table 1). Nonetheless, the combination of *Pparg*^ΔHep^ and TZD reduced the levels of ALT and liver weight and size and improved histology and steatosis to levels similar to those of LFCF-fed mice (Figure 8*B* and *C*). Furthermore, although TZD reduced *Timp1* expression in control mice, it reduced *Tnfa*, *Col1a1*, *Mmp13*, and *Timp1* expression, confirming the strong effect of the TZD treatment on the liver of HFCF-fed *Pparg*^ΔHep^ mice (Figure 8*D*).

Table 1. Plasma Levels of Lipids, Glucose, and Insulin in Control and *Pparg*^ΔHep^ Mice Fed LFCF Diet, HFCF Diet, or HFCF Diet With TZD

	LFCF diet						HFCF diet					
24 weeks HFCF	Control			*Pparg*^ΔHep^			Control			*Pparg*^ΔHep^		
TG, *mg/dL*	33.37	±	2.93	41.79	±	3.47	31.12	±	1.23	30.35^a^	±	2.98
NEFA, *mEq/L*	0.74	±	0.10	0.91	±	0.08	0.85	±	0.06	0.83	±	0.06
Cholesterol, *mg/dL*	183.46	±	12.51	165.01	±	11.58	240.51	±	13.10	248.20^b^	±	15.23
8 weeks HFCF												
Glucose, *mg/dL*	164.57	±	13.95	192.90	±	6.65	176.67	±	8.24	201.89	±	13.0
Insulin, *ng/mL*	0.680	±	0.119	0.805	±	0.098	1.407^a^	±	0.180	1.498^a^	±	0.144
24 weeks HFCF												
Glucose, *mg/dL*	179.71	±	4.91	158.00	±	9.60	176.17	±	4.99	187.38^a^	±	6.85
Insulin, *ng/mL*	1.52	±	0.21	1.88	±	0.29	1.16	±	0.07	2.37***	±	0.26
	HFCF diet						HFCF diet to HFCF/TZD diet					LFCF diet
Reversion	Control			*Pparg*^ΔHep^			Control			*Pparg*^ΔHep^		Control
Glucose, *mg/dL*	147.13^@^	±	7.95	181.29**	±	5.92	154.13	±	7.42	191.14**	±	3.87	175.43 ± 5.19
Insulin, *ng/mL*	0.66^@^	±	0.08	0.81	±	0.24	0.28	±	0.03	0.83*	±	0.07	1.63 ± 0.18

NOTE. Letters indicate differences induced by diet within group (control or *Pparg*^ΔHep^). @ indicates differences between LFCF- and HFCF-fed controls in the reversion study. *Asterisks* indicate differences between control and *Pparg*^ΔHep^ within diets. NFA, nonesterified fatty acid.
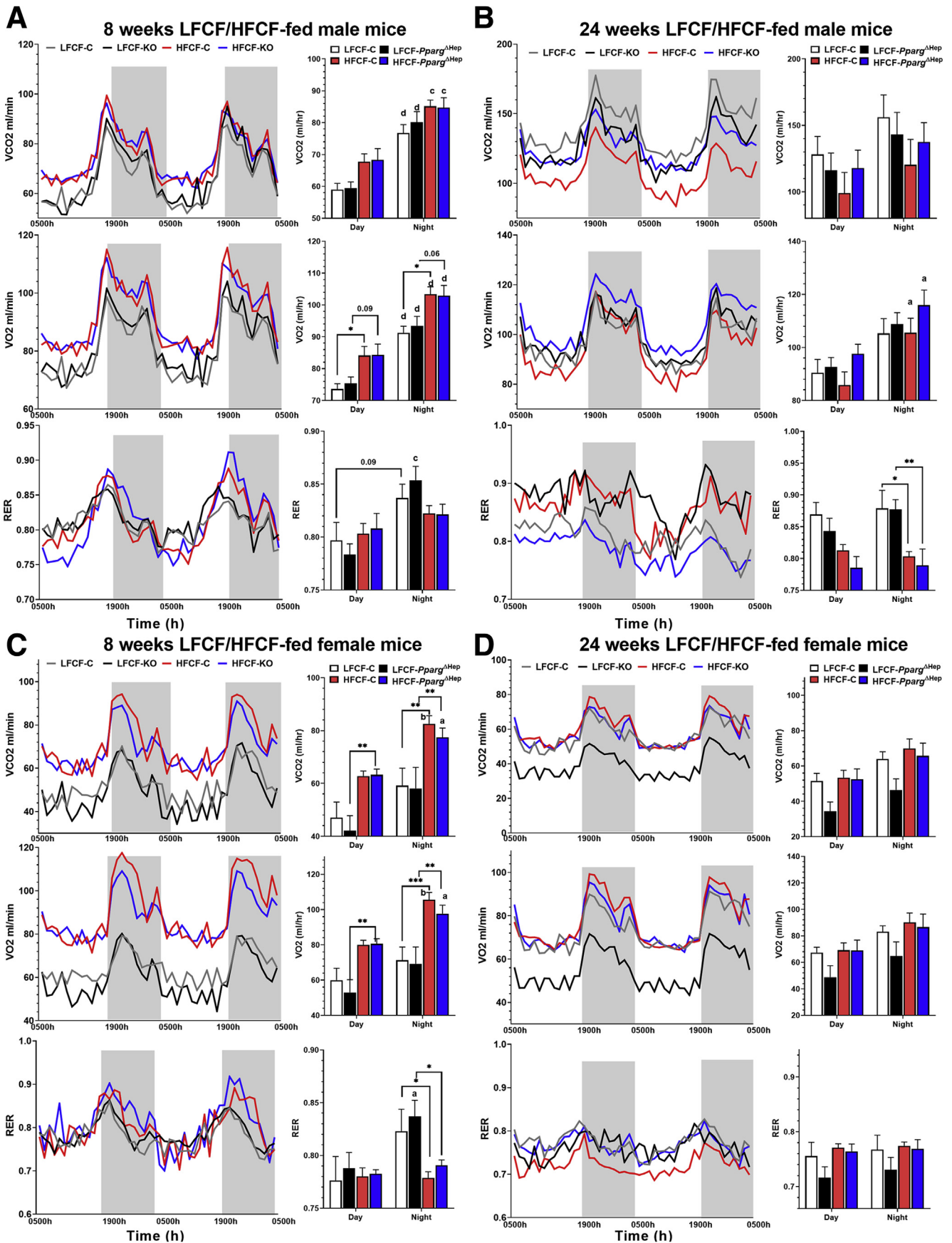^a,*,@^P < .05.
^b,**^P < .01.
***P < .001.

Figure 6. Plasma ALT and liver steatosis in control and *Pparg*$^{\Delta Hep}$ male mice fed LFCF or HFCF diet for 8 weeks. (*A*) Plasma ALT levels, (*B*) liver weight, and (*C*) liver TG content in male control and *Pparg*$^{\Delta Hep}$ mice. *Letters* indicate significant differences between LFCF- and HFCF-fed mice within group (C or KO), and *asterisks* indicate significant differences between control and *Pparg*$^{\Delta Hep}$ mice within diet. $^*P < .05$; $^bP < .01$; $^{c,***}P < .001$; $^dP < .0001$. n = 7–10 mice/group.
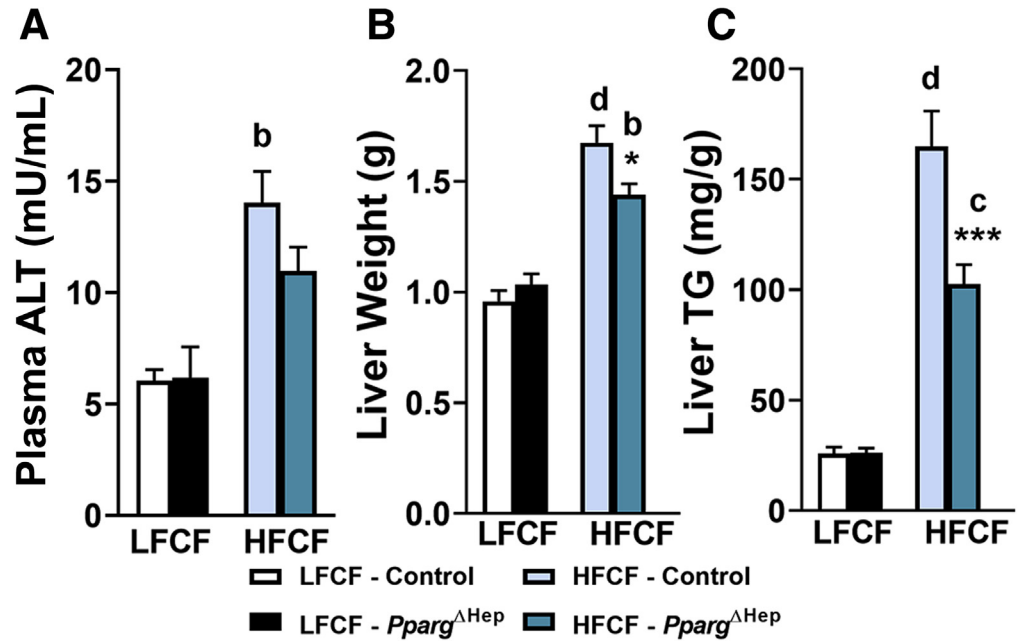
It should be noted that this short and low dose treatment of rosiglitazone increased insulin sensitivity but not adiposity in HFCF-fed control mice. However, in HFCF-fed *Pparg*$^{\Delta Hep}$ mice rosiglitazone dramatically increased body weight because of a selective expansion of adiposity (NMR-based fat mass and weight of white adipose tissues, Figure 9*A*–*C*). Although HFCF-fed mice did not show reduced NMR-based fat mass (as shown in Figure 2*A*), the expression of adipose tissue PPARγ and *Leptin* was reduced by HFCF diet (Figure 9*D*), which supports the negative impact of HFCF diet in adipose tissue biology. Interestingly, the expression of PPARγ, the PPARγ-responsive genes (*Cidec, Fabp4*), and adiponectin was increased in TZD-treated HFCF-fed *Pparg*$^{\Delta Hep}$ mice (Figure 9*D*). Furthermore, TZD increased the levels of plasma adiponectin, which were significantly elevated in HFCF-fed *Pparg*$^{\Delta Hep}$ mice (Figure 9*E*). Strikingly, the levels of hepatic phospho-AMPK, which are increased by adiponectin, were elevated in TZD-treated HFCF-fed *Pparg*$^{\Delta Hep}$ mice as compared with the levels of TZD in HFCF-fed control mice (Figure 9*F*). Taken together, these results suggest that TZD actions on adipocytes are enhanced because of the loss of hepatocyte PPARγ expression, and that has a strong effect in the activation of phospho-AMPK levels in the liver that could contribute to reduce steatosis.

To assess whether TZD actions in the liver of HFCF-fed *Pparg*$^{\Delta Hep}$ mice were altered to reduce NASH, we performed RNAseq in the livers of this cohort of mice (GEO #GSE162276). Similar to the previous cohort of mice shown in Figure 7, HFCF diet in control mice up-regulated GO terms related with fibrogenesis and inflammation and focal adhesion pathway, whereas it down-regulated those related with mitochondria metabolism (Figure 10*A*, Supplementary Data). Although TZD altered a similar number of DEGs in control and *Pparg*$^{\Delta Hep}$ mice, the impact of TZD on the liver transcriptome differed between control and *Pparg*$^{\Delta Hep}$ mice. In control mice with NASH, TZD positively regulated lipid metabolism and negatively amino acid metabolism. In contrast, TZD down-regulated GO terms and pathways related with immune response in *Pparg*$^{\Delta Hep}$ mice (Figure 10*B*, Supplementary Data), indicating that the anti-inflammatory properties of TZD were enhanced because of the loss of hepatocyte PPARγ expression. Next, we assessed the effect of *Pparg*$^{\Delta Hep}$ after HFCF-induced NASH. Independent of TZD, *Pparg*$^{\Delta Hep}$ altered the expression of 368 DEGs, but with TZD, *Pparg*$^{\Delta Hep}$ altered the expression of 1421 DEGs. This latter comparison suggested that TZD may differentially regulate the expression of hepatic gene expression in a hepatocyte PPARγ-dependent manner. Indeed, TZD strongly up-regulated amino acid metabolism and down-regulated inflammation in HFCF-fed *Pparg*$^{\Delta Hep}$ mice as compared with the effect of TZD in HFCF-fed control mice (Figure 10*C*, Supplementary Data). Taken together, hepatocyte PPARγ mediated the regulation of fatty acid

Figure 5. (*See previous page*). **Metabolic phenotype of control and *Pparg*$^{\Delta Hep}$ male (*top*) and female (*bottom*) mice.** The 48-hour curves and day/night averages of volume of O2 (VO2) (*top panels*), volume of CO2 (VCO2) (*central panels*), and respiratory exchange ratio (RER, *bottom panels*) in male mice fed LFCF or HFCF diet for 8 weeks (*A*) or 24 weeks (*B*) and female mice fed LFCF or HFCF diet for 8 weeks (*C*) or 24 weeks (*D*). *Letters* (a–d) indicate significant differences between day and night within group and diet (control, C and *Pparg*$^{\Delta Hep}$, KO). *Asterisks* indicate significant differences induced by HFCF within group in day or night period. $^{a,*,\#}P < .05$; $^{b,**}P < .01$; $^{c***}P < .001$; $^dP < .0001$. n = 7–8 mice/group in males, 5–11 mice/group in females.
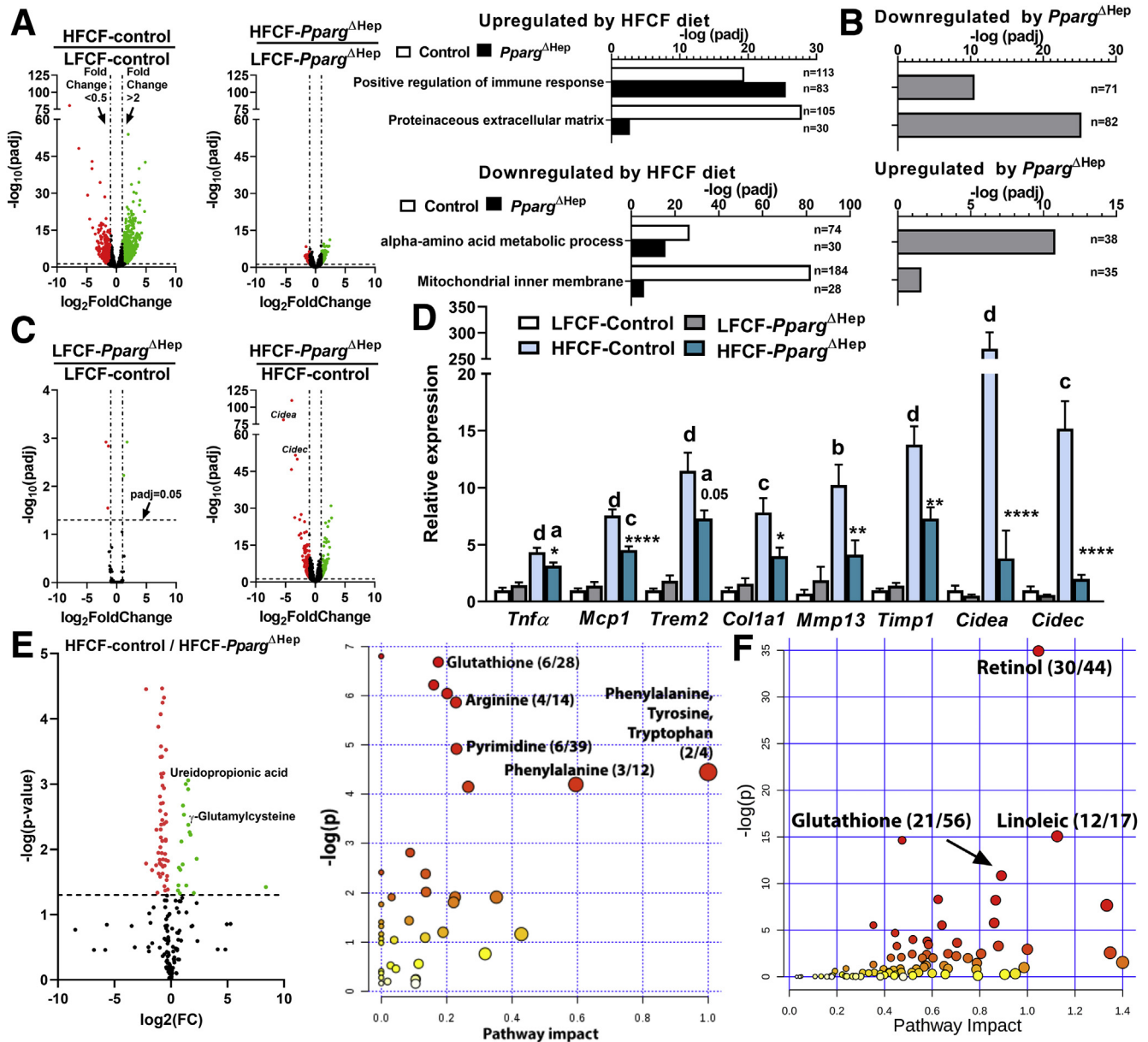
Figure 7. Hepatocyte PPARγ regulates hepatic metabolism associated with progression of NASH. RNAseq analysis of livers from control and Pparg^ΔHep male mice fed LFCF or HFCF diets for 24 weeks. (A) Volcano plot of hepatic DEGs and up-regulated and down-regulated GO terms by HFCF diet. (B) Pparg^ΔHep-mediated up-regulation and down-regulation of GO terms in HFCF-fed mice relative to HFCF-fed control mice. (C) Volcano plot of hepatic DEG regulated by hepatocyte Pparg^ΔHep in LFCF- and HFCF-fed mice. (D) Hepatic pro-inflamatory (Tnfa, Mcp1, Trem2), pro-fibrogenic (Col1a1, Mmp13, Timp1), and PPARγ-target (Cidea, Cidec) gene expression in LFCF- and HFCF-fed control and Pparg^ΔHep male mice. Letters indicate significant differences between LFCF- and HFCF-fed mice within group, and asterisks indicate significant differences between control and Pparg^ΔHep mice within diet. [a],*$P < .05$; [b],**$P < .01$; [c]$P < .001$; [d],****$P < .0001$. (E) Volcano plot and enrichment analysis of the 73 differentially regulated metabolites by Pparg^ΔHep in HFCF-fed mice. (F) Joint pathway analysis of the hepatic genes and metabolites regulated by Pparg^ΔHep in HFCF-fed mice. Number of hits/total number in pathways are indicated between parentheses. Green dots (up-regulated), red dots (down-regulated) DEG/differentially regulated metabolites. In A–C, E, and F, n = 4–5 mice/group. In D, n = 7–18 mice/group.

metabolism by TZD, which is one of the canonical pathways regulated by PPARγ, and Pparg^ΔHep enhanced the positive effects of TZD on inflammation and fibrogenesis and reduced those on amino acids metabolism.

The association between TZD, hepatocyte PPARγ, and hepatic gene pathways related to amino acid metabolism led us to measure the levels of hepatic metabolites. Interestingly, the differentially regulated metabolites identified from the comparison of HFCF-fed control and Pparg^ΔHep mice treated with TZD indicate that cysteine and methionine metabolism and pyrimidine metabolism are regulated by TZD in a hepatocyte PPARγ-dependent manner (Figure 10D,
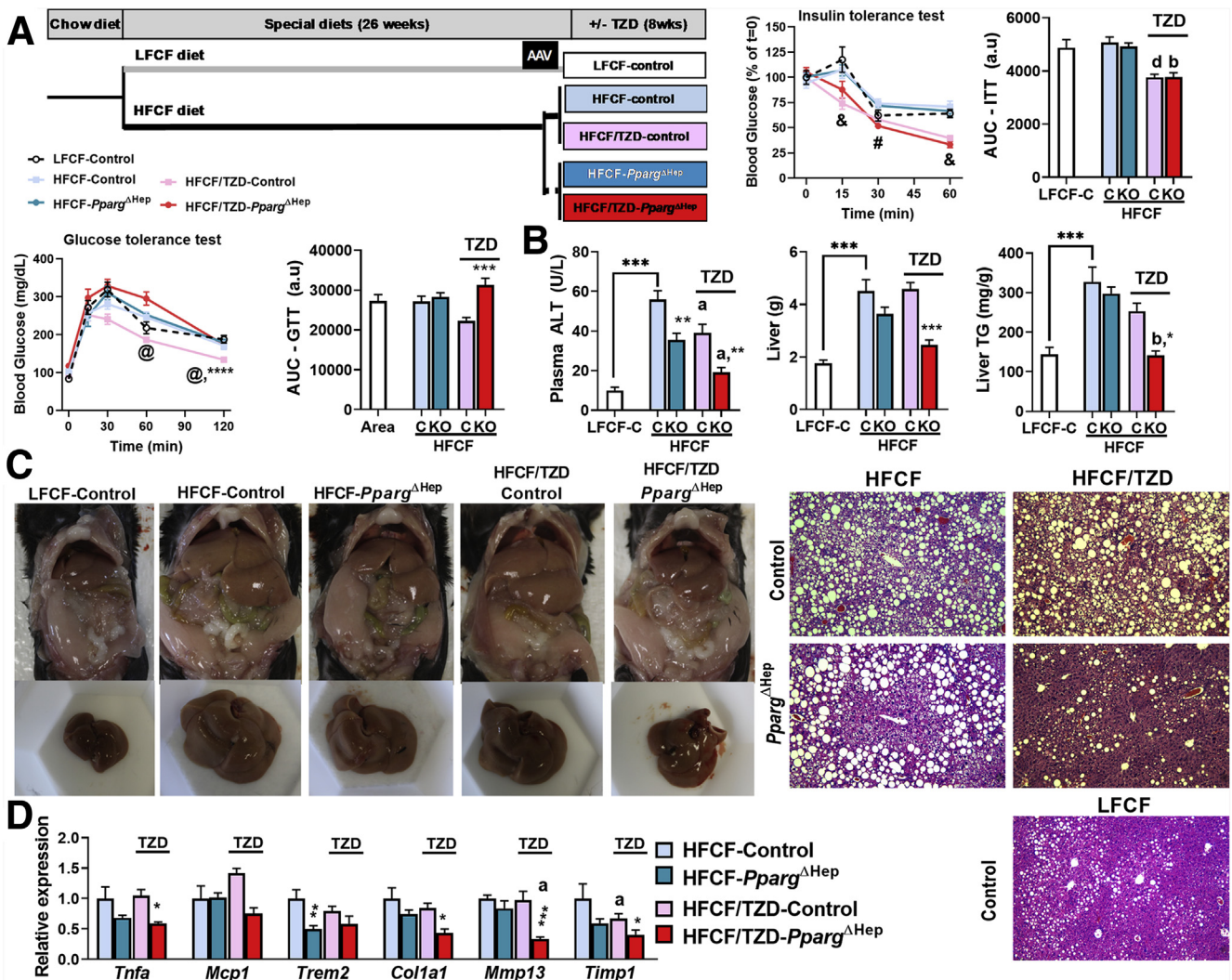
Figure 8. *Pparg*^ΔHep enhanced therapeutic effects of TZD on the liver. (*A*) 10- to 12-week-old male mice were fed LFCF or HFCF diet for 24 weeks and then treated with AAV to generate control and *Pparg*^ΔHep mice. Two weeks later, half of the HFCF-fed mice in each group were switched to HFCF diet with 50 mg/kg rosiglitazone maleate (TZD) for 8 additional weeks. After 7 weeks of TZD treatment, insulin tolerance test and glucose tolerance test were performed. (*B*) Plasma ALT, liver weight, and liver TG content. (*C*) Representative pictures of livers, and hematoxylin-eosin–stained liver sections of control mice fed LFCF diet or control and *Pparg*^ΔHep mice fed HFCF with and without TZD. (*F*) Hepatic pro-inflamatory (*Tnfa, Mcp1, Trem2*) and pro-fibrogenic (*Col1a1, Mmp13, Timp1*) gene expression in control and *Pparg*^ΔHep mice fed HFCF diet with and without TZD. *Letters* (a–d, @, #, &) indicate significant differences between HFCF- and HFCF/TZD-fed mice within group (control, C and *Pparg*^ΔHep, KO; @, only C; #, only KO; &, C and KO). *Asterisks* indicate significant differences between control and *Pparg*^ΔHep mice within diet. ^a,*,@,#,&*P* < .05; ^b,***P* < .01; ^c,****P* < .001; ^d,*****P* < .0001. AUC, area under the curve. n = 7–8 mice/group.

Supplementary Data). Furthermore, the combined analysis of RNAseq and metabolomics showed again that glutathione metabolism, retinol metabolism, and linoleic acid metabolism (Figure 10*D*, *right*) were regulated by TZD in a hepatocyte PPARγ-dependent manner as shown in Figure 7. Taken together, the results of these omics approaches in 2 different cohorts of mice support that the expression of PPARγ in hepatocytes alters the response to TZD in the liver with NASH and had a major effect in the regulation in the metabolism of hepatic amino acids, nucleotides, and lipids that contribute to sustain NASH.

The question that remained in our study was whether TZD could directly activate hepatocyte PPARγ in vivo after

the development of NASH. This is a relevant clinical question because it is commonly accepted that expression of hepatic PPARγ is reduced in NASH patients because of methylation of PPARγ promoter.[25] After 34 weeks of HFCF diet, the expression of hepatic PPARγ was not significantly increased in control mice as compared with their LFCF-fed littermates, and the TZD treatment did not increase hepatic PPARγ expression in HFCF-fed mice. However, PPARγ expression was reduced in *Pparg*^ΔHep mice, and the expression of PPARγ-target genes *Cidea, Cidec,* and *Cd36* was increased by TZD only in control (PPARγ-intact) mice (Figure 10*E*). In fact, the KEGG pathway PPAR signaling pathway was up-regulated by TZD in HFCF-fed control mice only (Supplementary Data).
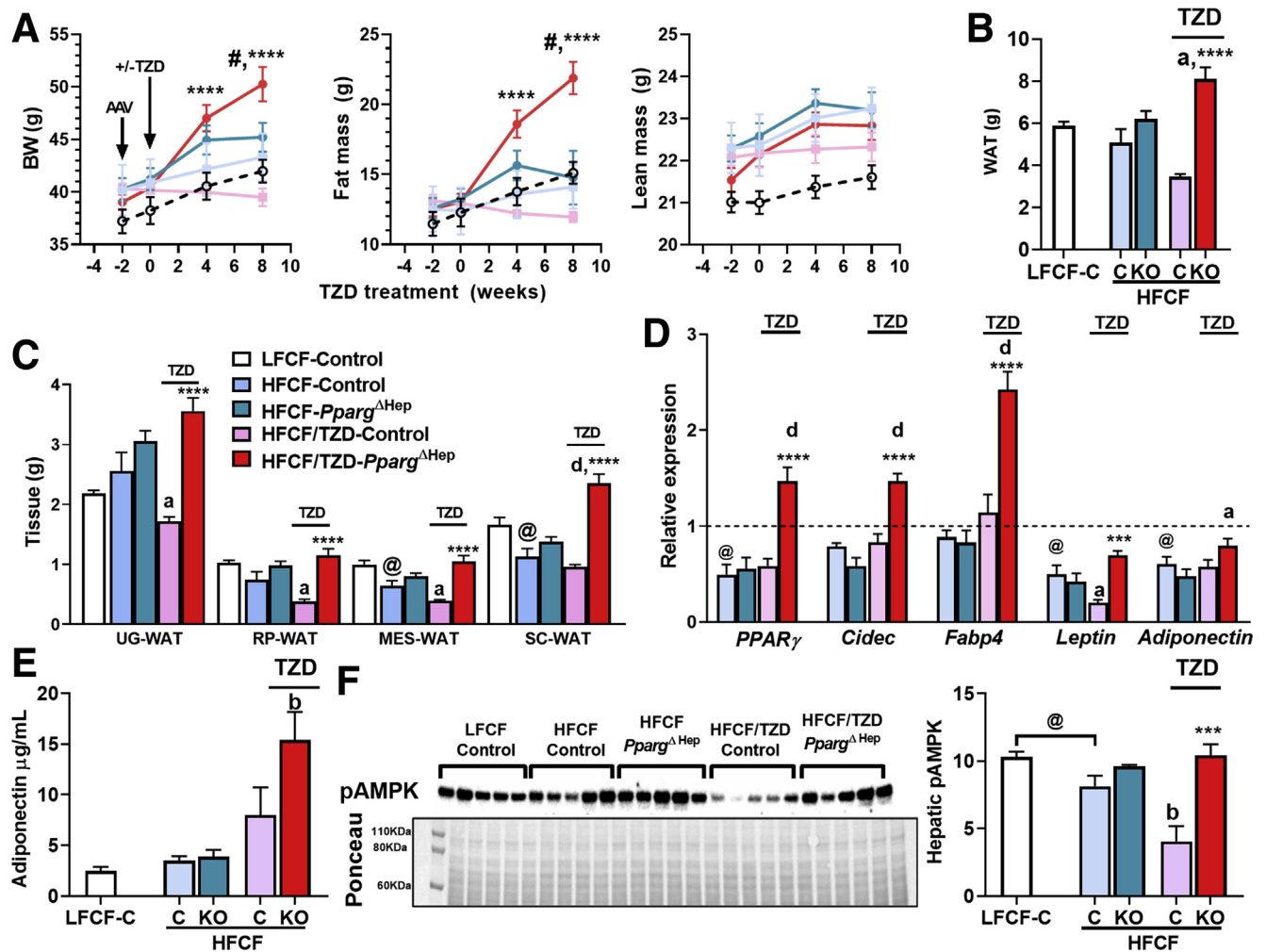
Figure 9. *Pparg*^ΔHep enhanced the effects of TZD on the adipose tissue. (*A*) Body weight (BW), NMR-based changes in fat mass and lean mass during TZD treatment. (*B*) Weight of white adipose tissue (WAT). (*C*) Weight of urogenital (UG), retroperitoneal (RP), mesenteric (MES), and subcutaneous (SC) WAT. (*D*) Gene expression of subcutaneous adipose tissue PPARγ, *Cidec*, fatty acid binding protein 4 (*Fabp4*), *Leptin*, and *Adiponectin*. Values are relative to those of LFCF-fed controls that are represented as a *dotted line*. (*E*) Plasma adiponectin levels. (*F*) Hepatic levels of phosphorylated AMPK normalized by Ponceau S staining. *Letters* (a–d, #) indicate significant differences induced by TZD within group (control, C or *Pparg*^ΔHep, KO; #, only KO mice). *Asterisks* indicate significant differences between control and *Pparg*^ΔHep mice within diet. @Significant differences between LFCF-fed control and HFCF-fed control (assessed by Student *t* test). $^{a,\#,@}P < .05$; $^{b,**}P < .01$; $^{***}P < .001$; $^{d,****}P < .0001$. n = 7–8 mice/group, n = 5 mice/group in (*F*).

Furthermore, rosiglitazone increased the expression of *Cidec* and *Cd36* and tended to increase hepatocyte *Cidea* only in mouse primary hepatocytes isolated from PPARγ-intact mice with NASH (Figure 10*F*). Taken together, TZD show differential effects in *Pparg*^ΔHep vs control mice and have enhanced effects on extrahepatic tissues and non-parenchymal cells of the liver to reduce NASH because of the loss of hepatocyte PPARγ expression.

Hepatocyte-Specific Loss of PPARγ Positively Regulates Methionine Metabolism in Mice Fed a HFCF Diet

The liver metabolizes most of dietary methionine to produce S-adenosylmethionine (SAM) via methionine adenosyltransferase 1a or to synthesize proteins.[26] SAM donates methyl groups to methyltransferases and is converted into S-adenosylhomocysteine (SAH). Then, SAH-hydrolase (AHCY) converts SAH into homocysteine (Hcy), which is used to produce glutathione or re-methylated to methionine by betaine-homocysteine methyltransferase (BHMT)[27] (Figure 11*A*). Interestingly, the levels of the metabolites of the methionine cycle including methionine, SAM, SAH, and Hcy were regulated by HFCF diet or TZD (Supplementary Data). In addition, the expression of *Mat1a*, phosphatidylethanolamine methyltransferase (*Pemt*), glycine N-methyltransferase (*Gnmt*), nicotinamide N-methyltransferase (*Nnmt*), *Ahcy*, and *Bhmt* was reduced in HFCF-fed control mice (Figure 11*B*), as previously described in GEO: GSE119340.[28] Interestingly, the expression of *Pemt* and *Bhmt* was not significantly reduced in HFCF-fed *Pparg*^ΔHep mice, which suggests that PPARγ is a negative

regulator of these genes (Figure 11*B*). Also, HFCF-fed mice displayed elevated levels of hepatic Hcy consistent with a previous report,[29] whereas SAM and Met levels were increased in HFCF-fed *Pparg*$^{\Delta\text{Hep}}$ mice (Figure 11*C*). Overall, these results confirmed that methionine cycle was disrupted in HFCF-fed mice, and hepatocyte PPARγ expression may be contributing to the negative effect of HFCF diet on methionine metabolism.

TZD treatment in HFCF-fed control mice did not downregulate the expression of the genes of methionine cycle as compared with non-treated HFCF-fed control littermates. However, in HFCF-fed *Pparg*$^{\Delta\text{Hep}}$ mice, TZD increased the expression of hepatic *Pemt, Gnmt, Nnmt,* and *Ahcy* to levels similar to those in LFCF-fed controls (Figure 11*D*). Furthermore, the expression of hepatic *Bhmt* was enhanced by TZD in *Pparg*$^{\Delta\text{Hep}}$ mice, and this was associated with a dramatic reduction of Hcy and betaine levels (Figure 11*E*). Also, the levels of hepatic SAH, the common product of the hepatic methyltransferases, was increased in HFCF-fed *Pparg*$^{\Delta\text{Hep}}$ mice treated with TZD (Figure 11*E*), suggesting that the activity of methyltransferases of the methionine cycle was restored. Overall, our data indicate that *Pparg*$^{\Delta\text{Hep}}$ reduces the impact of HFCF diet on methionine cycle, and this allows for the restoration of genes and metabolites of the methionine cycle because of the benefits derived from the treatment with TZD in extrahepatic tissues and in non-parenchymal cells.

Discussion

The hepatocyte-specific knockout of PPARγ before and after the development of NASH showed that hepatocyte PPARγ contributes to the progression of NASH and reduces the benefits derived from the effects of rosiglitazone on extrahepatic tissues and non-parenchymal cells, respectively, in mice with NASH. The hepatocyte-specific contribution of PPARγ to the progression of NASH is based on the improved hepatic condition shown by HFCF-fed *Pparg*$^{\Delta\text{Hep}}$ mice with and without TZD treatment, which was concomitant with impaired glucose metabolism and obesity, both common features of patients with NAFLD. In addition, the combination of different unbiased omics approaches in 2 different experiments indicated that HFCF diet alters lipid, nucleotide, and amino acid metabolism in the liver in a hepatocyte PPARγ-dependent manner and suggested that these processes contribute to the progression of NASH.

Our experimental approach showed that >90% of liver PPARγ expression is hepatocyte-specific.[18,30] Hepatic PPARγ expression is low in lean mice, but it increases upon feeding with a high-fat diet and contributes to the development of steatosis.[17–19,31,32] In mice with liver steatosis, a short-term treatment with a low dose of TZD, 50–100 mg rosiglitazone/kg of diet, which represents a daily dose of 3–5 mg/kg body weight, promotes steatosis in a hepatocyte PPARγ-dependent manner. In fact, the loss of hepatocyte PPARγ expression enhances the anti-steatogenic effects of rosiglitazone.[19,32] Similarly, a long-term treatment with a low dose of rosiglitazone in diet-induced obese mice with compromised PPARγ function (constitutive deacetylated

isoform of PPARγ) reduces steatosis, but the effect was not evident in diet-induced obese mice.[33] Accordingly, in this study, rosiglitazone reduced liver steatosis, reversed NASH, and increased adiposity in HFCF-fed *Pparg*$^{\Delta\text{Hep}}$ mice but not in control mice. Our results indicate that loss of hepatocyte PPARγ expression enhances the actions of TZD in extrahepatic tissues (insulin sensitizing in adipose tissue) and in the non-parenchymal cells of the liver (anti-inflammatory in macrophages, anti-fibrogenic in hepatic stellate cells) to reverse NASH efficiently. Because we knocked out PPARγ only in hepatocytes, our data further support that endogenous or TZD-mediated activation of PPARγ in hepatocytes may alter the therapeutic effects of TZD on the liver in a model of NASH. However, the mechanisms regulated by hepatocyte PPARγ that promote and sustain steatosis, as well as their contribution in the development of NASH, remain unknown.

PPARγ promotes DNL and fatty acid uptake in hepatocytes.[16–19] In fact, genetic ablation of hepatocyte PPARγ in different models of diet-induced steatosis with and without alcohol consumption reduces steatosis, the expression of genes involved in DNL, fatty acid uptake and re-esterification, ALT levels, and fibrosis in a mouse model-dependent manner.[17–19,34,35] Of note, in a model of fast food diet-induced NASH, the pharmacologic inhibition of epidermal growth factor receptor reduced the transcriptional activity of PPARγ and the expression of genes involved in DNL genes,[36] as well as fibrosis. From these studies, we could assume that the steatogenic effects of PPARγ may promote the development of NAFLD. However, we did not see major significant changes of steatogenic genes in HFCF-fed mice, and the reduction of HFCF-induced steatosis in *Pparg*$^{\Delta\text{Hep}}$ mice was modest. In addition, we published that *Pparg*$^{\Delta\text{Hep}}$ does not reduce steatosis in a model of DNL-mediated steatosis[37] or in a model of steatohepatitis induced by methionine- and choline-deficient diet, but rather, it reduces fibrosis.[30] Therefore, the steatogenic role of hepatocyte PPARγ and its contribution to the development of NASH is mouse model- and diet-dependent. However, growing evidence supports a positive association between hepatocyte PPARγ and fibrosis.[30,34,36] In this sense, our unbiased transcriptomic analysis revealed that *Pparg*$^{\Delta\text{Hep}}$ had a major impact in the regulation of pathways related with inflammation and fibrogenesis rather than steatosis, which strongly suggests that the presence and activation of hepatocyte PPARγ may be relevant in the activation of non-parenchymal cells during the progression of NAFLD.

Our omics approaches also revealed that hepatic methionine metabolism is altered in HFCF-fed mice in a hepatocyte PPARγ-dependent manner. The disruption of methionine metabolism in the liver may promote NASH[26] because the methionine cycle provides methyl groups to lipids, nucleotides, and proteins required to maintain hepatocyte physiology. In particular, PEMT is mostly expressed in hepatocytes, and it is a key enzyme of the methionine cycle that methylates phosphatidylethanolamine to phosphatidylcholine, accounting for 30% of production of hepatic phosphatidylcholine. The knockout of PEMT promotes NASH in mice because of the reduction of

phosphatidylcholine that impairs the production of very low density lipoprotein.[38] BHMT is primarily expressed in hepatocytes and plays a major role in the remethylation of Hcy to methionine. The knockout of BHMT promotes NAFLD because of increased levels of hepatic Hcy that can lead to hepatocyte damage.[39] The translational relevance of our
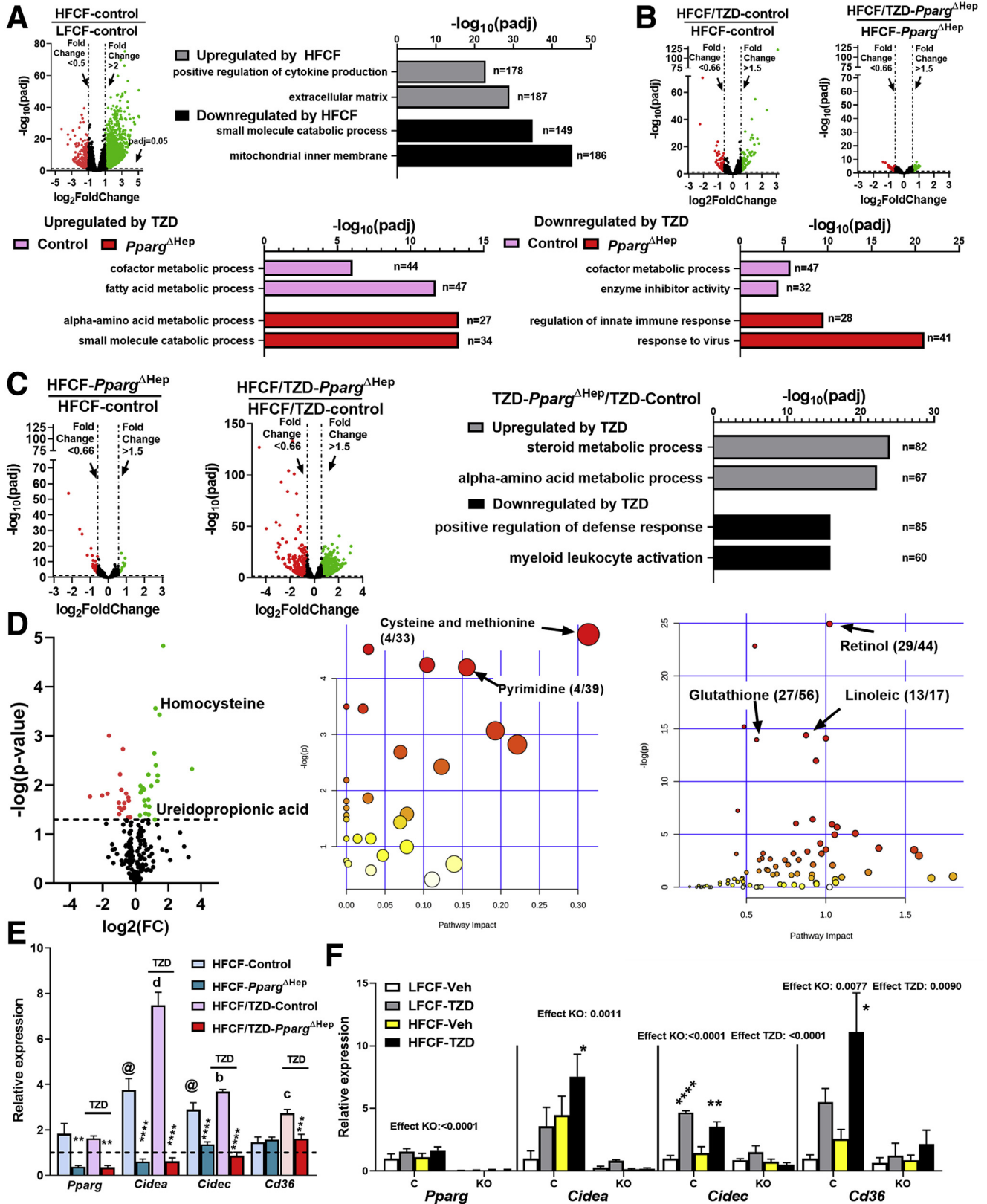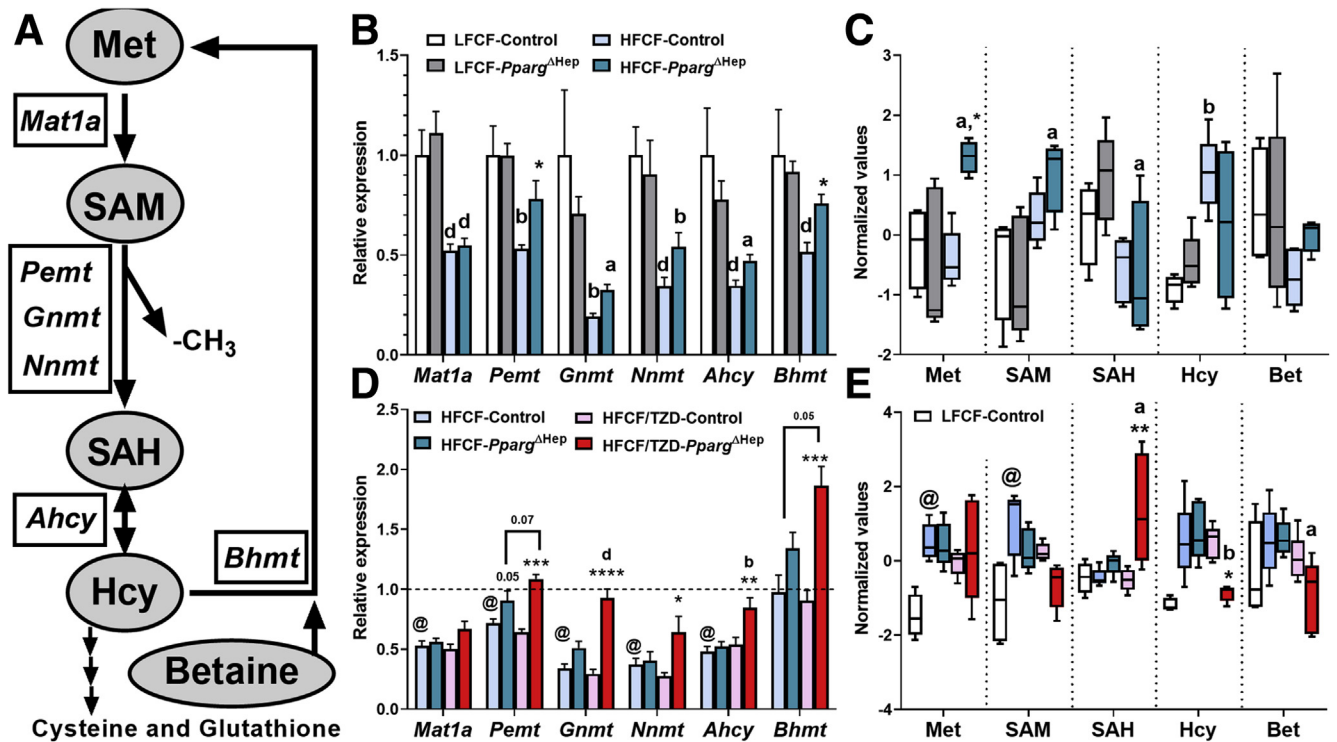
Figure 11. Hepatocyte PPARγ negatively regulates methionine homeostasis in NASH. (A) Scheme of selected metabolites (*ovals*) and gene (*squares*) of the methionine cycle. (B) Hepatic gene expression and (C) normalized levels of metabolites of the methionine cycle in livers of LFCF- and HFCF-fed control and *Pparg*^ΔHep^ mice. (D) Hepatic gene expression and (E) normalized levels of metabolites of methionine in LFCF-fed control (*dotted line*, set at 1 in *D*, and *open box* in *E*) and HFCF- and HFCF/TZD-fed control and *Pparg*^ΔHep^ male mice. *Letters* (a–d) indicate significant differences between HFCF- and HFCF/TZD-fed mice within group (control and *Pparg*^ΔHep^). @Difference between LFCF- and HFCF-fed control mice. *Asterisks* indicate significant differences between control and *Pparg*^ΔHep^ mice within diet. ᵃ,*,@,&$P < .05$; ᵇ,**$P < .01$; ᶜ,***$P < .001$; ᵈ,****$P < .0001$. n = 4–5 mice/group.

observations relies on the fact that rosiglitazone can reduce hepatic PEMT activity,[40] patients with NASH show reduced PEMT and BHMT levels,[41,42] as well as single nucleotide polymorphisms associated with reduced enzymatic activity of PEMT and BHMT,[42,43] which may alter the levels of metabolites of the methionine cycle. Reduced expression and/or activity of PEMT and BHMT contribute to the accumulation of Hcy and lipids in the liver without altering lipid metabolism (lipogenesis) and subsequently promote cytotoxic events.[43] Therefore, the up-regulation of *Pemt* and *Bhmt* expression in the liver of *Pparg*^ΔHep^ indicates that hepatocyte PPARγ plays a negative role in the regulation of

methionine cycle that leads to the accumulation of fat and promotes the development of hepatocyte damage during NASH progression.

TZD have been used to reverse NASH in humans on the basis of their anti-inflammatory and anti-fibrogenic properties in macrophages and hepatic stellate cells, respectively,[10] and insulin sensitizing properties in adipose tissue.[44] TZD are promising drugs for the treatment of NAFLD because they have positive effects on ALT levels, steatosis, inflammation, and hepatocyte ballooning as summarized in several meta-analyses of specific clinical trials (<24 months).[45–47] Long-term treatments (24–40 months)

Figure 10. (*See previous page*). **Activation of hepatocyte PPARγ with TZD in NASH alters hepatic metabolism.** (A) Volcano plot and enrichment analysis of hepatic DEGs regulated by 34 weeks of HFCF diet in control mice. (B) Volcano plot and enrichment analysis of hepatic DEGs regulated by TZD treatment in HFCF-fed control and *Pparg*^ΔHep^ male mice. (C) Volcano plot and enrichment analysis of hepatic DEGs regulated by *Pparg*^ΔHep^ in mice fed HFCF diet with TZD. (D) Volcano plot (*left*), enrichment analysis (*middle*), and joint pathway analysis (*right*) of the 40 differentially regulated metabolites by *Pparg*^ΔHep^ in mice fed HFCF diet with TZD. Number of hits/total number in pathways are indicated between parentheses. Expression of hepatic PPARγ and PPARγ-target genes *Cidea, Cidec*, and *Cd36* in (E) LFCF-fed control (*dotted line*, set at 1) and HFCF- and HFCF/TZD-fed control and *Pparg*^ΔHep^ male mice and in (F) mouse primary hepatocytes isolated from control and *Pparg*^ΔHep^ mice fed LFCF and HFCF diet for 29–31 weeks and treated with 50 μmol/L rosiglitazone for 24 hours. @Difference between LFCF- and HFCF-fed control mice. *Letters* (a–d) indicate significant differences between HFCF- and HFCF/TZD-fed mice within group (control and *Pparg*^ΔHep^). *Asterisks* indicate significant differences between control and *Pparg*^ΔHep^ mice within diet. ᵃ,*,@,&$P < .05$; ᵇ,**$P < .01$; ᶜ,***$P < .001$; ᵈ,****$P < .0001$. n = 7–8 mice/group. padj, adjusted *P* value.

with pioglitazone and rosiglitazone increased insulin sensitivity in patients with NASH and reduced steatosis.[4–6] However, the FLIRT2 trial described an "exhaustion of the antisteatogenic effect" of rosiglitazone, which could be associated to the maximal effect of insulin sensitization of rosiglitazone.[5] The PIVENS trial also requested caution in the interpretation of the results of pioglitazone on NASH.[6] Recently, a trial that used pioglitazone in NASH patients improved liver histology after 18 months of treatment, but the extension of the study did not promote additional reductions in steatosis.[4] Similarly, in mice fed a HFCF diet, long-term treatment with pioglitazone increased insulin sensitivity and partially reduced liver steatosis[48] but did not reduce steatosis in mice with preexisting NASH.[49] Strikingly, this study shows that the true potential of TZD as a therapy for NASH is reduced in control (PPARγ-intact) mice. Our results indicate that hepatocyte PPARγ regulates molecular mechanisms in hepatocytes beyond those related with lipid metabolism, which could contribute to sustain NASH and reduce the positive effects derived from the TZD-mediated activation of PPARγ in extrahepatic tissues and non-parenchymal cells of the liver. These mechanisms may differ from the classical lipogenic mechanisms (DNL, fatty acid uptake) that PPARγ regulates in adipose tissue and muscle and may include the maintenance of methionine homeostasis in hepatocytes, which is a key mechanism to prevent hepatocyte damage, and the activation of non-parenchymal cells in the liver that ultimately are responsible for the development of NASH. Although this study used rosiglitazone maleate, future studies could assess whether hepatocyte PPARγ reduces the therapeutic actions of pioglitazone hydrochloride.

In conclusion, our study highlights that hepatocyte-specific loss of PPARγ protects mice from diet-induced NASH and enhances the positive effects of TZD on NASH. Therefore, the inhibition of PPARγ activity specifically in hepatocytes or the blockage of mechanisms driven by hepatocyte PPARγ in the liver that offset the therapeutic effects of anti-NASH drugs will increase the efficiency of TZD and other therapies in the reversion of NASH.

Methods

Mouse Model

All mouse studies were approved by the Institutional Animal Care and Use Committee of the University of Illinois at Chicago, and they were performed in accordance with guidelines and regulations of the University of Illinois at Chicago. Pparg^{fl/fl} mice[50] were purchased from Jackson Laboratories (Strain 004584, B3.129-Ppargtm2Rev/J; Bar Harbor, ME) and bred as homozygotes in a temperature (22°C–24°C) and humidity controlled specific-pathogen free barrier facility with 14-hour light/10-hour dark cycle (lights on at 6:00 AM) in the Biologic Resources Laboratory of the University of Illinois at Chicago. Pparg[ΔHep] mice were generated by injecting 100 μL saline containing 1.5×10^{11} genome copies of AAV serotype 8 (AAV8) vectors that bear a thyroxine binding globulin (TBG)-driven Cre recombinase (AAV8-TBG-Cre; Penn Vector Core, University of

Pennsylvania) in the lateral-tail vein of Pparg^{fl/fl} mice.[18,30] We described the hepatocyte-specific expression of transgene delivered by AAV-TBG vectors previously.[18,51] A subset of Pparg^{fl/fl} littermate mice injected with 1.5×10^{11} genome copies of AAV8-TBG-Null generates controls. Two weeks after AAV injections, half of the chow-fed mice in each group were fed the LFCF (Cat # D09100304) or the HFCF (Cat #D16010101; Research Diets, Inc, New Brunswick) diets for 24 weeks. These mice were used to generate results of Figures 1–7 and 11B and C. In a second cohort of HFCF-fed mice, 2 weeks after generation of control and Pparg[ΔHep] mice, half of the mice in each group were fed the HFCF diet or the HFCF diet with 50 mg rosiglitazone maleate/kg (Cat #D1808030; Research Diets) for 8 additional weeks. Rosiglitazone maleate was purchased from AdipoGen Life Sciencies (San Diego, CA).

Body Composition, Glucose Homeostasis, and Metabolic Rate

Whole-body fat, lean, and fluid mass were measured with a minispec LF50 Body Composition Analyzer (Bruker, Billerica, MA). Glucose (2 mg glucose intraperitoneal [ip]/g in males, 1 mg glucose ip/g in females) and pyruvate (2 mg sodium pyruvate ip/g) tolerance tests were performed in overnight fasted mice. Insulin tolerance test (1–1.5 mU insulin ip/g in males, 0.75 mU insulin ip/g in females) was performed in mice after 4-hour food withdrawal at 7:00 AM. Blood glucose was measured from lateral tail vein with glucometer (Accu-check; Roche, Basel, Switzerland). Energy expenditure, volume of oxygen utilization, carbon dioxide output, respiratory exchange ratio, food intake, and activity were measured by using Promethion Systems (Sable Systems International, Las Vegas, NV) and analyzed with calR software on the basis of total mass (Metabolic Core, Beth Israel Deaconess Medical Center, Boston, MA).[52]

Metabolic Endpoints Measured in Plasma

Several groups of mice were killed by decapitation 4 hours after food withdrawal at 7:00 AM, and trunk blood was collected from the site where the animal was decapitated into EDTA-coated microtainers (BD, Franklin Lakes, NJ) and kept in ice until centrifugation to separate plasma. Plasma was used to determine levels of nonesterified fatty acid, TG, cholesterol (Wako Diagnostics, Richmond, VA), insulin (Mercodia, Uppsala, Sweden), adiponectin (Abcam, Cambridge, MA), and ALT (Pointe Scientific, Canton, MI). To assess hepatic TG content, hepatic lipids were extracted from frozen livers in isopropanol, and TG was measured as previously published.[37]

Histology and Pathology Assessment

Formalin-fixed livers were processed by the Research Histology and Tissue Imaging Core of the University of Illinois at Chicago and stained with hematoxylin-eosin or picrosirius red/fast green.[30] Pathologic features of the liver sections were graded in a blinded fashion following the scoring system of Kleiner et al.[53]

RNAseq and Quantitative Polymerase Chain Reaction

RNA was extracted using Trizol Reagent (Life Technologies, Carlsbad, CA) and used to perform RNAseq or quantitative polymerase chain reaction as previously described.[54–56] Sequences of the primers used for quantitative polymerase chain reaction are described in Supplementary Data. Libraries preparation, sequencing, and bioinformatics analysis of RNAseq were performed by Novogen (Novogen, Inc, Sacramento CA). Briefly, RNA integrity was assessed with Agilent Bioanalyzer 2100 to select RNA samples with RIN >7.3 to 9.3. Two hundred fifty to 300 base pair insert cDNA libraries, non–strand-specific, were prepared with New England Biolabs (Ipswich, MA) Next Ultra RNA Library Prep and sequenced with Illumina (San Diego, CA) HiSeq PE150 Platform ∼6G/sample Q30 >90%. The reads were mapped to the mouse reference genome sequence (GRCm38/mm10) using STAR v2.5 and v2.6.1, with a total mapping rate >90%/sample. For gene expression level analysis and to calculate the fragments per kilobase of transcript per million mapped reads, HTSeq v0.6.1 was used. The differential expression analysis between 2 different groups was done with DESeq2 R package v2_1.6.3. The P values were adjusted using the Benjamini-Hochberg approach for controlling the false discovery rate, adjusted $P < .05$. TFCat and Cosmic databases were used to annotate the differential expressed gene. The enrichment analysis (GO and KEGG) was done with cluster Profiler R package. Tables generated in the analysis of these RNAseq experiments are provided as Supplementary Data. The high-throughput sequencing data from this study have been published in GEO with the accession numbers GSE162249 and GSE162276.

Western Blot

Livers were homogenized with beads in a tissue homogenizer (Next Advance, Troy, NY) in RIPA buffer (Sigma-Aldrich) supplemented with protease inhibitor (Complete; Roche) and phosphatase inhibitor cocktails (Sigma-Aldrich), followed by centrifugation to obtain protein in supernatants. Protein was quantified with BCA protein assay kit (Thermo Fisher Scientific, Waltham, MA), and equal amounts of proteins were heated in Laemmli sample buffer with dithiothreitol at 95°C for 5–10 minutes. Twenty μg protein/well separated in 26-well Criterion TGX stain-free gels at 200 V in Tris-glycine–sodium dodecyl sulfate buffer and transferred onto nitrocellulose membranes using a Bio-Rad Turbo Transfer system (Bio-Rad Laboratories, Hercules, CA). We stained the membranes with Ponceau S staining for protein normalization, and membranes were scanned with a Bio-Rad Gel Doc system (Bio-Rad Laboratories). Then, Ponceau S staining was washed out, membranes were blocked for 1 hour at 25°C with 5% nonfat dry milk in Tris-buffered saline with 0.05% Tween-20, washed, and incubated overnight at 4°C with phosphorylated AMPK 1/1000 (#50081; Cell Signaling Technology, Danvers, MA). Finally, membranes were washed and incubated for 1 hour at 25°C with goat anti-rabbit immunoglobulin G (H + L)–

horseradish peroxidase conjugate, 1/2000 (Bio-Rad Laboratories). After washing, Immobilon Western Chemiluminiscent horseradish peroxidase substrate (Millipore Sigma, Burlington, MA) was added, and the light signal was detected with a Bio-Rad Gel Doc system (Bio-Rad Laboratories). Bands were quantified with ImageJ software (National Institutes of Health, Bethesda, MD).

Mouse Primary Hepatocytes

A group of control and $Pparg^{\Delta Hep}$ mice that were fed a LFCF or HFCF diet for 29–31 weeks were anesthetized with ketamine/xylazine and killed by exsanguination during liver perfusion. The liver was perfused with 40 mL of wash buffer (137 mmol/L NaCl, 7 mmol/L KCl, 0.7 mmol/L Na2HPO4, 10 mmol/L HEPES, 0.5 mmol/L EDTA, pH = 7.65) at 37°C at 6–8 mL/min, followed by 40 mL of digestion buffer (0.01% collagenase type I from *Clostridium histolyticum* (Sigma-Aldrich; C5138), 137 mmol/L NaCl, 7 mmol/L KCl, 0.7 mmol/L Na2HPO4, 10 mmol/L HEPES, 5 mmol/L CaCI2, pH = 7.65) at 37°C at 6–8 mL/min. When digestion was completed, the liver was dissected from the mouse, the gallbladder was removed, and the liver was gently resuspended in ice-cold complete M199 medium (10% fetal bovine serum, 2 mmol/L L-glutamine, 10 nmol/L insulin, 500 nmol/L dexamethasone, 1× penicillin-streptomycin). Then, the hepatocytes were filtered using 70 μm nylon strainers and centrifuged at 100*g* for 3 minutes. The supernatant was then aspirated, and the pellet was washed with fresh ice-cold complete M199 medium and centrifuged at 100*g* for 3 minutes 3 times. Hepatocytes were plated on 12-well cell culture plates precoated with type I rat tail collagen (Corning, Corning, NY) at a density of 200,000 cells/well and placed in a cell culture incubator at 37°C, 5% CO_2. After 4 hours of recovery, the medium was replaced with culture M199 medium (5% fetal bovine serum, 2 mmol/L L-glutamine, 100 nmol/L dexamethasone, 1× penicillin-streptomycin) for an overnight incubation at 37°C, 5% CO_2. Next day, hepatocytes were washed in serum-free culture M199 medium and cultured with and without 50 μmol/L rosiglitazone (Sigma-Aldrich) for 24 hours at 37°C in a 5% CO_2 incubator.

Steady-State Metabolomics

Fifty milligrams of frozen liver was homogenized in 80% Ultrapure HPLC grade methanol (Fisher Scientific) and 20% Ultrapure water (Fisher Scientific) on dry ice. After centrifugation, the pellet was resuspended in 8 mol/L urea, proteins were quantified with BCA protein assay kit (Thermo Fisher Scientific), and the supernatant was dried up under nitrogen for 6 hours. Then, dried metabolites were resuspended in 50% liquid chromatography-mass spectrometry grade acetonitrile at a final concentration of 20 μg protein/ μL. Samples were processed by the Metabolomics Core Facility at Robert H. Lurie Comprehensive Cancer Center of Northwestern University with high-performance liquid chromatography and high-resolution mass spectrometry and tandem mass spectrometry.[57] Briefly, 10 μL of sample

was separated with a Xbridge Amide column (Waters) and a gradient mobile phase with a flow rate of 400 μL/min of solution A (95:5 parts of water/acetonitrile, 20 mmol/L ammonium hydroxide, 20 mmol/L ammonium acetate, pH = 9) and solution B (acetonitrile) as follows: 0 minutes, 15% A; 2.5 minutes, 30% A; 7 minutes, 43% A; 16 minutes, 62% A; 16.1–18 minutes, 75% A; 18–25 minutes, 15% A. The temperature of the electrospray ionization capillary was set to 275°C and the spray voltage at 4.0 kV, with the mass spectrometry in positive/negative polarity switching mode. An m/z scan range from 70 to 850 was chosen, and MS1 data were collected at a resolution of 70,000. The top 5 precursor ions were subsequently fragmented in a data-dependent manner by using the higher energy collisional dissociation cell set to 30% normalized collision energy in MS2 at a resolution power of 17,500. Data acquisition and analysis were carried out by Xcalibur 4.0 software and Tracefinder 2.1 software, respectively (Thermo Fisher Scientific). Analysis of the 189 hydrophilic metabolites identified in our panel was performed with MetaboAnalyst software.[58] Tables generated in the analysis of these metabolomics experiments are provided in Supplementary Data.

Statistical Analysis

Values are represented as means $\pm$ standard errors of the mean. Data were analyzed by 2-way analysis of variance followed by a Tukey or Bonferroni post hoc test, or Student t test when applicable. Metabolic cages data obtained from CalR were analyzed by two-way analysis of variance followed by Bonferroni post hoc tests. Analysis of RNAseq data and enrichment analysis of DEG were performed by Novogen, Inc. Differentially regulated metabolites and enrichment analysis of metabolomics were performed with MetaboAnalyst software.[58] The statistical analyses were performed by using GraphPad Prism 8 (GraphPad Software, La Jolla, CA). P values less than .05 were considered significant.

All authors had access to the study data and had reviewed and approved the final manuscript.

References

1. Portillo-Sanchez P, Bril F, Maximos M, Lomonaco R, Biernacki D, Orsak B, Subbarayan S, Webb A, Hecht J, Cusi K. High prevalence of nonalcoholic fatty liver disease in patients with type 2 diabetes mellitus and normal plasma aminotransferase levels. J Clin Endocrinol Metab 2015;100:2231–2238.
2. Younossi ZM, Tampi RP, Racila A, Qiu Y, Burns L, Younossi I, Nader F. Economic and clinical burden of nonalcoholic steatohepatitis in patients with type 2 diabetes in the United States. Diabetes Care 2020;43:283–289.
3. Friedman SL, Neuschwander-Tetri BA, Rinella M, Sanyal AJ. Mechanisms of NAFLD development and therapeutic strategies. Nat Med 2018;24:908–922.
4. Cusi K, Orsak B, Bril F, Lomonaco R, Hecht J, Ortiz-Lopez C, Tio F, Hardies J, Darland C, Musi N, Webb A, Portillo-Sanchez P. Long-term pioglitazone treatment for patients with nonalcoholic steatohepatitis and prediabetes or type 2 diabetes mellitus: a randomized trial. Ann Intern Med 2016;165:305–315.
5. Ratziu V, Charlotte F, Bernhardt C, Giral P, Halbron M, Lenaour G, Hartmann-Heurtier A, Bruckert E, Poynard T, Group LS. Long-term efficacy of rosiglitazone in nonalcoholic steatohepatitis: results of the fatty liver improvement by rosiglitazone therapy (FLIRT 2) extension trial. Hepatology 2010;51:445–453.
6. Sanyal AJ, Chalasani N, Kowdley KV, McCullough A, Diehl AM, Bass NM, Neuschwander-Tetri BA, Lavine JE, Tonascia J, Unalp A, Van Natta M, Clark J, Brunt EM, Kleiner DE, Hoofnagle JH, Robuck PR, Nash CRN. Pioglitazone, vitamin E, or placebo for nonalcoholic steatohepatitis. N Engl J Med 2010;362:1675–1685.
7. Harrison SA, Alkhouri N, Davison BA, Sanyal A, Edwards C, Colca JR, Lee BH, Loomba R, Cusi K, Kolterman O, Cotter G, Dittrich HC. Insulin sensitizer MSDC-0602K in non-alcoholic steatohepatitis: a randomized, double-blind, placebo-controlled phase IIb study. J Hepatol 2020;72:613–626.
8. Azzu V, Vacca M, Virtue S, Allison M, Vidal-Puig A. Adipose tissue-liver cross talk in the control of whole-body metabolism: implications in nonalcoholic fatty liver disease. Gastroenterology 2020;158:1899–1912.
9. Ahmadian M, Suh JM, Hah N, Liddle C, Atkins AR, Downes M, Evans RM. PPARgamma signaling and metabolism: the good, the bad and the future. Nat Med 2013;19:557–566.
10. Moran-Salvador E, Titos E, Rius B, Gonzalez-Periz A, Garcia-Alonso V, Lopez-Vicario C, Miquel R, Barak Y, Arroyo V, Claria J. Cell-specific PPARgamma deficiency establishes anti-inflammatory and anti-fibrogenic properties for this nuclear receptor in non-parenchymal liver cells. J Hepatol 2013; 59:1045–1053.
11. Pettinelli P, Videla LA. Up-regulation of PPARgamma mRNA expression in the liver of obese patients: an additional reinforcing lipogenic mechanism to SREBP-1c induction. J Clin Endocrinol Metab 2011;96:1424–1430.
12. Lima-Cabello E, Garcia-Mediavilla MV, Miquilena-Colina ME, Vargas-Castrillon J, Lozano-Rodriguez T, Fernandez-Bermejo M, Olcoz JL, Gonzalez-Gallego J, Garcia-Monzon C, Sanchez-Campos S. Enhanced expression of pro-inflammatory mediators and liver X-receptor-regulated lipogenic genes in non-alcoholic fatty liver disease and hepatitis C. Clin Sci (Lond) 2011; 120:239–250.
13. Jia X, Zhai T. Integrated analysis of multiple microarray studies to identify novel gene signatures in non-alcoholic fatty liver disease. Front Endocrinol (Lausanne) 2019; 10:599.
14. Chella Krishnan K, Kurt Z, Barrere-Cain R, Sabir S, Das A, Floyd R, Vergnes L, Zhao Y, Che N, Charugundla S, Qi H, Zhou Z, Meng Y, Pan C, Seldin MM, Norheim F, Hui S, Reue K, Lusis AJ, Yang X. Integration of multi-omics data from mouse diversity panel highlights mitochondrial

dysfunction in non-alcoholic fatty liver disease. Cell Syst 2018;6:103–115 e7.

15. de Conti A, Tryndyak V, Willett RA, Borowa-Mazgaj B, Watson A, Patton R, Khare S, Muskhelishvili L, Olson GR, Avigan MI, Cerniglia CE, Ross SA, Sanyal AJ, Beland FA, Rusyn I, Pogribny LP. Characterization of the variability in the extent of nonalcoholic fatty liver induced by a high-fat diet in the genetically diverse Collaborative Cross mouse model. FASEB J 2020;34:7773–7785.

16. Gavrilova O, Haluzik M, Matsusue K, Cutson JJ, Johnson L, Dietz KR, Nicol CJ, Vinson C, Gonzalez FJ, Reitman ML. Liver peroxisome proliferator-activated receptor gamma contributes to hepatic steatosis, triglyceride clearance, and regulation of body fat mass. J Biol Chem 2003;278:34268–34276.

17. Moran-Salvador E, Lopez-Parra M, Garcia-Alonso V, Titos E, Martinez-Clemente M, Gonzalez-Periz A, Lopez-Vicario C, Barak Y, Arroyo V, Claria J. Role for PPARgamma in obesity-induced hepatic steatosis as determined by hepatocyte- and macrophage-specific conditional knockouts. FASEB J 2011; 25:2538–2550.

18. Wolf Greenstein A, Majumdar N, Yang P, Subbaiah PV, Kineman RD, Cordoba-Chacon J. Hepatocyte-specific, PPARgamma-regulated mechanisms to promote steatosis in adult mice. J Endocrinol 2017;232:107–121.

19. Matsusue K, Haluzik M, Lambert G, Yim SH, Gavrilova O, Ward JM, Brewer B Jr, Reitman ML, Gonzalez FJ. Liver-specific disruption of PPARgamma in leptin-deficient mice improves fatty liver but aggravates diabetic phenotypes. J Clin Invest 2003;111:737–747.

20. Yu S, Matsusue K, Kashireddy P, Cao WQ, Yeldandi V, Yeldandi AV, Rao MS, Gonzalez FJ, Reddy JK. Adipocyte-specific gene expression and adipogenic steatosis in the mouse liver due to peroxisome proliferator-activated receptor gamma1 (PPARgamma1) overexpression. J Biol Chem 2003;278:498–505.

21. Gaskell H, Ge X, Desert R, Das S, Han H, Lantvit D, Guzman G, Nieto N. Ablation of Hmgb1 in intestinal epithelial cells causes intestinal lipid accumulation and reduces NASH in mice. Hepatol Commun 2020; 4:92–108.

22. Chiappini F, Coilly A, Kadar H, Gual P, Tran A, Desterke C, Samuel D, Duclos-Vallee JC, Touboul D, Bertrand-Michel J, Brunelle A, Guettier C, Le Naour F. Metabolism dysregulation induces a specific lipid signature of nonalcoholic steatohepatitis in patients. Sci Rep 2017;7:46658.

23. Mantena SK, King AL, Andringa KK, Eccleston HB, Bailey SM. Mitochondrial dysfunction and oxidative stress in the pathogenesis of alcohol- and obesity-induced fatty liver diseases. Free Radic Biol Med 2008; 44:1259–1272.

24. Pettinelli P, Arendt BM, Teterina A, McGilvray I, Comelli EM, Fung SK, Fischer SE, Allard JP. Altered hepatic genes related to retinol metabolism and plasma retinol in patients with non-alcoholic fatty liver disease. PLoS One 2018;13:e0205747.

25. Hardy T, Zeybel M, Day CP, Dipper C, Masson S, McPherson S, Henderson E, Tiniakos D, White S, French J, Mann DA, Anstee QM, Mann J. Plasma DNA methylation: a potential biomarker for stratification of liver fibrosis in non-alcoholic fatty liver disease. Gut 2017;66:1321–1328.

26. Mato JM, Martinez-Chantar ML, Lu SC. S-adenosylmethionine metabolism and liver disease. Ann Hepatol 2013;12:183–189.

27. Chen NC, Yang F, Capecci LM, Gu Z, Schafer AI, Durante W, Yang XF, Wang H. Regulation of homocysteine metabolism and methylation in human and mouse tissues. FASEB J 2010;24:2804–2817.

28. Xiong X, Wang Q, Wang S, Zhang J, Liu T, Guo L, Yu Y, Lin JD. Mapping the molecular signatures of diet-induced NASH and its regulation by the hepatokine Tsukushi. Mol Metab 2019;20:128–137.

29. Pacana T, Cazanave S, Verdianelli A, Patel V, Min HK, Mirshahi F, Quinlivan E, Sanyal AJ. Dysregulated hepatic methionine metabolism drives homocysteine elevation in diet-induced nonalcoholic fatty liver disease. PLoS One 2015;10:e0136822.

30. Cordoba-Chacon J. Loss of hepatocyte-specific PPAR-gamma expression ameliorates early events of steatohepatitis in mice fed the methionine and choline-deficient diet. PPAR Res 2020;2020:9735083.

31. Inoue M, Ohtake T, Motomura W, Takahashi N, Hosoki Y, Miyoshi S, Suzuki Y, Saito H, Kohgo Y, Okumura T. Increased expression of PPARgamma in high fat diet-induced liver steatosis in mice. Biochem Biophys Res Commun 2005;336:215–222.

32. Chao L, Marcus-Samuels B, Mason MM, Moitra J, Vinson C, Arioglu E, Gavrilova O, Reitman ML. Adipose tissue is required for the antidiabetic, but not for the hypolipidemic, effect of thiazolidinediones. J Clin Invest 2000;106:1221–1228.

33. Kraakman MJ, Liu Q, Postigo-Fernandez J, Ji R, Kon N, Larrea D, Namwanje M, Fan L, Chan M, Area-Gomez E, Fu W, Creusot RJ, Qiang L. PPARgamma deacetylation dissociates thiazolidinedione's metabolic benefits from its adverse effects. J Clin Invest 2018;128:2600–2612.

34. Wang W, Xu MJ, Cai Y, Zhou Z, Cao H, Mukhopadhyay P, Pacher P, Zheng S, Gonzalez FJ, Gao B. Inflammation is independent of steatosis in a murine model of steatohepatitis. Hepatology 2017; 66:108–123.

35. Zhang W, Sun Q, Zhong W, Sun X, Zhou Z. Hepatic peroxisome proliferator-activated receptor gamma signaling contributes to alcohol-induced hepatic steatosis and inflammation in mice. Alcohol Clin Exp Res 2016;40:988–999.

36. Bhushan B, Banerjee S, Paranjpe S, Koral K, Mars WM, Stoops JW, Orr A, Bowen C, Locker J, Michalopoulos GK. Pharmacologic inhibition of epidermal growth factor receptor suppresses nonalcoholic fatty liver disease in a murine fast-food diet model. Hepatology 2019;70:1546–1563.

37. Kineman R, Majumdar N, Subbaiah PV, Cordoba-Chacon J. Hepatic PPARγ is not essential for the rapid

development of steatosis following loss of hepatic GH signaling, in adult male mice. Endocrinology 2016; 157:1728–1735.

38. Nakatsuka A, Matsuyama M, Yamaguchi S, Katayama A, Eguchi J, Murakami K, Teshigawara S, Ogawa D, Wada N, Yasunaka T, Ikeda F, Takaki A, Watanabe E, Wada J. Insufficiency of phosphatidylethanolamine N-methyltransferase is risk for lean non-alcoholic steatohepatitis. Sci Rep 2016;6:21721.

39. Teng YW, Mehedint MG, Garrow TA, Zeisel SH. Deletion of betaine-homocysteine S-methyltransferase in mice perturbs choline and 1-carbon metabolism, resulting in fatty liver and hepatocellular carcinomas. J Biol Chem 2011;286:36258–36267.

40. Pan HJ, Reifsnyder P, Vance DE, Xiao Q, Leiter EH. Pharmacogenetic analysis of rosiglitazone-induced hepatosteatosis in new mouse models of type 2 diabetes. Diabetes 2005;54:1854–1862.

41. Zhu X, Song J, Mar MH, Edwards LJ, Zeisel SH. Phosphatidylethanolamine N-methyltransferase (PEMT) knockout mice have hepatic steatosis and abnormal hepatic choline metabolite concentrations despite ingesting a recommended dietary intake of choline. Biochem J 2003;370(Pt 3):987–993.

42. Kalhan SC, Edmison J, Marczewski S, Dasarathy S, Gruca LL, Bennett C, Duenas C, Lopez R. Methionine and protein metabolism in non-alcoholic steatohepatitis: evidence for lower rate of transmethylation of methionine. Clin Sci (Lond) 2011;121:179–189.

43. Radziejewska A, Muzsik A, Milagro FI, Martinez JA, Chmurzynska A. One-carbon metabolism and nonalcoholic fatty liver disease: the crosstalk between nutrients, microbiota, and genetics. Lifestyle Genom 2020; 13:53–63.

44. Soccio RE, Chen ER, Lazar MA. Thiazolidinediones and the promise of insulin sensitization in type 2 diabetes. Cell Metab 2014;20:573–591.

45. Boettcher E, Csako G, Pucino F, Wesley R, Loomba R. Meta-analysis: pioglitazone improves liver histology and fibrosis in patients with non-alcoholic steatohepatitis. Aliment Pharmacol Ther 2012;35:66–75.

46. He L, Liu X, Wang L, Yang Z. Thiazolidinediones for nonalcoholic steatohepatitis: a meta-analysis of randomized clinical trials. Medicine (Baltimore) 2016; 95:e4947.

47. Musso G, Cassader M, Paschetta E, Gambino R. Thiazolidinediones and advanced liver fibrosis in nonalcoholic steatohepatitis: a meta-analysis. JAMA Intern Med 2017;177:633–640.

48. Kalavalapalli S, Bril F, Koelmel JP, Abdo K, Guingab J, Andrews P, Li WY, Jose D, Yost RA, Frye RF, Garrett TJ, Cusi K, Sunny NE. Pioglitazone improves hepatic mitochondrial function in a mouse model of nonalcoholic steatohepatitis. Am J Physiol Endocrinol Metab 2018; 315:E163–E173.

49. Kumar DP, Caffrey R, Marioneaux J, Santhekadur PK, Bhat M, Alonso C, Koduru SV, Philip B, Jain MR, Giri SR, Bedossa P, Sanyal AJ. The PPAR alpha/gamma agonist saroglitazar improves insulin resistance and steatohepatitis in a diet induced animal model of nonalcoholic fatty liver disease. Sci Rep 2020;10, ARTN 9330.

50. He W, Barak Y, Hevener A, Olson P, Liao D, Le J, Nelson M, Ong E, Olefsky JM, Evans RM. Adipose-specific peroxisome proliferator-activated receptor gamma knockout causes insulin resistance in fat and liver but not in muscle. Proc Natl Acad Sci U S A 2003; 100:15712–15717.

51. Cordoba-Chacon J, Majumdar N, List EO, Diaz-Ruiz A, Frank SJ, Manzano A, Bartrons R, Puchowicz M, Kopchick JJ, Kineman RD. Growth hormone inhibits hepatic de novo lipogenesis in adult mice. Diabetes 2015;64:3093–3103.

52. Mina AI, LeClair RA, LeClair KB, Cohen DE, Lantier L, Banks AS. CalR: a Web-based analysis tool for indirect calorimetry experiments. Cell Metab 2018;28:656–666 e1.

53. Kleiner DE, Brunt EM, Van Natta M, Behling C, Contos MJ, Cummings OW, Ferrell LD, Liu YC, Torbenson MS, Unalp-Arida A, Yeh M, McCullough AJ, Sanyal AJ. Nonalcoholic steatohepatitis clinical research, design and validation of a histological scoring system for nonalcoholic fatty liver disease. Hepatology 2005; 41:1313–1321.

54. Cordoba-Chacon J, Gahete MD, McGuinness OP, Kineman RD. Differential impact of selective GH deficiency and endogenous GH excess on insulin-mediated actions in muscle and liver of male mice. Am J Physiol Endocrinol Metab 2014;307:E928–E934.

55. Cordoba-Chacon J, Sarmento-Cabral A, Del Rio-Moreno M, Diaz-Ruiz A, Subbaiah PV, Kineman RD. Adult-onset hepatocyte GH resistance promotes NASH in male mice, without severe systemic metabolic dysfunction. Endocrinology 2018;159:3761–3774.

56. Sarmento-Cabral A, Del Rio-Moreno M, Vazquez-Borrego MC, Mahmood M, Guiterrez-Casado E, Pelke N, Guzman G, Subbaiah PV, Cordoba-Chacon J, Yakar S, Kineman RD. GH directly inhibits steatosis and liver injury in a sex-dependent and IGF1-independent manner. J Endocrinol 2021;248:31–44.

57. Ali ES, Sahu U, VillaE, O'Hara BP, Gao P, Beaudet C, Wood AW, Asara JM, Ben-Sahra I. ERK2 phosphorylates PFAS to mediate posttranslational control of de novo purine synthesis. Mol Cell 2020;78:1178–1191.

58. Chong J, Xia J. Using MetaboAnalyst 4.0 for metabolomics data analysis, interpretation, and integration with other omics data. Methods Mol Biol 2020;2104:337–360.

Correspondence

Address correspondence to: Jose Cordoba-Chacon, PhD, Department of Medicine, Section of Endocrinology, Diabetes and Metabolism, 835 South Wolcott Avenue (North Entrance), Suite E625, M/C 640, Chicago, Illinois 60612. fax (312) 413-0437. e-mail: jcordoba@uic.edu.

CRediT Authorship Contributions

Samuel Lee (Formal analysis: Equal; Investigation: Equal; Supervision: Equal; Writing – review & editing: Supporting)

Carolina Pusec (Formal analysis: Equal; Investigation: Equal; Writing – review & editing: Equal)

Gregory Norris (Formal analysis: Equal; Investigation: Equal; Writing – review & editing: Equal)

Adam De Jesus (Formal analysis: Equal; Investigation: Supporting; Writing – review & editing: Supporting)

Alberto Diaz-Ruiz (Formal analysis: Supporting; Investigation: Supporting; Writing – review & editing: Supporting)

Jose Muratalla (Formal analysis: Supporting; Investigation: Supporting; Writing – review & editing: Supporting)

Andre Sarmento-Cabral (Formal analysis: Supporting; Investigation: Supporting; Writing – review & editing: Supporting)

Grace Guzman (Formal analysis: Supporting; Investigation: Supporting)

Brian Layden (Conceptualization: Supporting; Writing – original draft: Supporting; Writing – review & editing: Supporting),

Jose Cordoba-Chacon, PhD (Conceptualization: Lead; Data curation: Lead; Formal analysis: Lead; Funding acquisition: Lead; Investigation: Lead; Methodology: Lead; Project administration: Lead; Supervision: Lead; Writing – original draft: Lead; Writing – review & editing: Lead)